Green Chemistry

TUTORIAL REVIEW

View Article Online
View Journal | View Issue



Cite this: *Green Chem.*, 2025, **27**, 4898



# Machine learning-driven design of single-atom catalysts for carbon dioxide valorization to high-value chemicals: a review of photocatalysis, electrocatalysis, and thermocatalysis

Xiangyu Wen, [a,b] Xiao Geng,[b] Guandong Su,[b,c] Yizheng Li, [d] Qidong Li,[e] Yuxuan Yi [f] and Lifen Liu *[b,c]

Received 11th February 2025,
Accepted 6th March 2025

DOI: 10.1039/d5gc00739a

rsc.li/greenchem

The pressing need for carbon-neutral technologies has driven extensive research into photocatalytic, electrocatalytic, and thermocatalytic $CO_2$ reduction, with highly efficient single-atom catalysts (SACs) due to their atomically dispersed active sites, tunable coordination environments, and well-defined electronic structures. Recent advances in SACs have demonstrated enhanced activity, selectivity and stability through rational design strategies incorporating transition-metal-based single-atom sites, nitrogen-coordinated frameworks, and perovskite-, graphene-, or MOF-supports. Mechanistically, SACs facilitate $CO_2$ activation *via* optimized $CO_2$ adsorption, electronic-state modulation and selective stabilization of key intermediates, thus promoting tailored product formation. Despite significant progress, challenges remain in understanding the precise electronic effects governing intermediate binding and selectivity and suppressing metal aggregation under operando conditions. This review systematically integrates experimental findings with machine learning (ML)-assisted first-principles calculations, deep learning (DL) frameworks, and density functional theory (DFT) modeling to refine the performances of SACs. ML-driven Bayesian optimization accelerates catalyst discovery by correlating the synthesis parameters with reaction kinetics and thermodynamics. High-throughput experimental validation combined with multi-technique characterization elucidates the structure–activity relationships, providing insights into the electron transfer dynamics, coordination tuning, and catalytic site evolution. The integration of active learning algorithms enables self-optimizing SACs, dynamically adjusting synthesis and reaction conditions for superior selectivity and faradaic efficiency. By bridging predictive modeling with experimental validation, this review presents a comprehensive framework for the rational design of next-generation SACs, paving the way for high-efficiency conversion of $CO_2$ into valuable chemicals. The synergy between AI-driven catalyst discovery and mechanistic elucidation represents a paradigm shift toward viable and selective $CO_2$ valorization strategies.

## Green foundation

1. This review discusses advancements in green chemistry, particularly in the $CO_2$ reduction reaction ($CO_2RR$) using single-atom catalysts (SACs). Key developments include the use of SACs for photocatalysis, electrocatalysis, and thermocatalysis, with improved $CO_2$ activation, enhanced selectivity, and increased efficiency through atomic-level precision.
2. The integration of experimental techniques with machine learning (ML), deep learning models (DL), and DFT establishes a data-driven framework for optimizing the design of SACs. This approach facilitates the iterative refinement of the catalyst properties, prediction of reaction pathways, and enhancement of efficiency and selectivity, thereby generating wider interest.
3. The future of this field lies in achieving a comprehensive understanding of mechanisms and refining SAC design through ML/DL/DFT and experimental validation. These insights will guide the rational development of SACs with enhanced performance, aiding the scalability of $CO_2$ reduction technologies and contributing to sustainability.

[a]*State Key Laboratory of Chemical Engineering, Zhejiang University, 310027 Hangzhou, China*
[b]*Key Laboratory of Industrial Ecology and Environmental Engineering (MOE), Dalian University of Technology, 116024 Liaoning, China. E-mail: lifenliu@dlut.edu.cn*
[c]*Department of Environment and Food, School of Chemical Engineering, Ocean, and Life Sciences, Dalian University of Technology, Panjin, 124221, China*
[d]*Department of Building Environment and Energy Engineering, The Hong Kong Polytechnic University, 999077 Hong Kong, China*
[e]*School of Engineering, The University of British Columbia, BC V1 V 1 V7, 1137 Alumni Ave, Kelowna, Canada*
[f]*College of Design and Engineering, National University of Singapore, 117575, Singapore*

# 1 Introduction

Rapid industrialization has greatly increased $CO_2$ emissions, intensifying the greenhouse effect and creating various social, ecological and environmental challenges. China's rising share in global emissions has spurred efforts for "dual carbon" goals, emphasizing the need for effective solutions like catalytic $CO_2$ reduction technologies. These technologies enable $CO_2$ conversion into valuable small organic molecules *via* thermocatalysis, electrocatalysis,[1–4] and photocatalysis,[5] offering promising pathways for $CO_2$ capture, storage (CCS), and utilization (CCU).[6,7] Thermocatalysis at high temperatures can activate $CO_2$, breaking C–O bonds and thereby producing $C_1$ and $C_2$ products. Meanwhile, in electrocatalysis,[8,9] $CO_2$ gets electrochemically reduced to form intermediates like formate, CO and methane;[10] in photocatalysis,[11] which mimics photosynthesis, light energy is used to generate charge carriers to activate and reduce $CO_2$.[12] These last two methods offer efficient solutions under mild conditions to reduce $CO_2$ emissions.[13] Converting $CO_2$ into high-value chemicals, such as CO, $CH_4$, HCOOH and $C_2$ compounds, is both a carbon utilization strategy and a focus area of $CO_2$RR for academic and industrial researchers.[14] The related progress is shown in the pivotal role of catalytic science and technology in driving advances in energy, environmental and industrial sectors, enhancing reaction efficiency and selectivity and lowering activation energies.[15] In recent years, the rapid progress of nanotechnology has propelled "nanocatalysts" to the forefront of energy, chemical, and environmental engineering owing to their high surface areas and unique catalytic properties.[16,17] Catalysts are designed to reduce the size of active metal components and to unveil the distinct catalytic effects at the nano-, sub-nano- and SAC-scale.[18] The concept of SACs was introduced while creating a $Pt_1/FeO_x$ catalyst, where a single platinum atom was anchored on a ferrite nanocrystal.

SACs offer distinct advantages over traditional nanocatalysts, including exceptionally high atomic efficiency, large surface areas and well-defined, uniform active sites. These properties make SACs highly effective in catalytic applications such as organocatalysis,[19,20] photocatalysis[21,22] and electrocatalysis.[23,24] In $CO_2$RR, SACs, especially those incorporating Co, N and C (*e.g.*, M–N–C), exhibit superior performance due to their tailored coordination environments, enhanced electronic properties and precise control over the active site geometry. The high reactivity of these materials stems from their ability to fine-tune the electronic structure and optimize the catalytic pathway, facilitating efficient $CO_2$ activation and reduction to small organic molecules such as CO, formate, and methane. The mechanism involving $CO_2$ adsorption, activation *via* metal sites, electron transfer and bond cleavage, and formation of specific products, is determined by the catalyst's electronic structure and the reaction conditions.[25] Despite significant progress in the design of high-density, high-stability SACs, the underlying mechanisms and their transformation during reactions remain poorly understood. While SACs theoretically maximize atomic efficiency, the increased surface energy of the isolated metal atoms, due to their higher surface area, can lead to aggregation under reaction conditions. As the metal loading increases, SACs tend to cluster, leading to a loss of catalytic performance. Therefore, achieving both high stability and large substrate loading in SACs remains a major challenge. This issue is particularly relevant in $CO_2$RR, where maintaining the integrity of the isolated metal sites is crucial for efficient $CO_2$ activation and selective reduction to organic molecules. Hence, solutions for optimizing support materials, such as nitrogen-doped carbon frameworks, to stabilize isolated metal sites and prevent aggregation while maintaining their high reactivity and selectivity for $CO_2$RR[26] are highly desirable.

Prediction and optimization of SACs using ML have become key research directions, with recent major advancements in ML offering powerful tools for accelerating catalyst discovery,[27]

**Xiangyu Wen**

*Mr Xiangyu Wen is currently pursuing a Master's degree in Chemical Engineering (Hydrogen Energy Science and Engineering) at Zhejiang University. His undergraduate research at Dalian University of Technology in 2024 focused on photocatalysis, electrocatalysis, and photoelectrocatalytic $CO_2$ reduction. Presently, his research is centered on the use of machine learning for catalyst design and thermocatalytic $CO_2$ reduction to produce high-value chemicals, with a commitment to advancing CCUS (Carbon Capture, Utilization, and Storage) and clean energy technologies.*

**Guandong Su**

*Dr Guandong Su is an Assistant Professor in the Department of Environment and Food, School of Chemical Engineering, Ocean, and Life Sciences, Dalian University of Technology. He received his PhD in Environmental Engineering from the National University of Singapore and B.Eng. in Petroleum Engineering from China University of Petroleum-Beijing in 2024 and 2018, respectively. His research interests lie in the interdisciplinary interface of energy and environment to advance sustainable development goals, with an emphasis on providing affordable and clean energy for the future.*

fine-tuning reaction parameters, and unveiling complex reaction pathways.[28,29] A key advancement in photocatalysis is the development of NiNi heterobimetallic SACs, which outperform traditional catalysts by utilizing a redox-active ligand for $CO_2$ activation, highlighting the importance of dual-metal cooperation in catalyst design.[30] In electrocatalysis, ML-guided DFT calculations have optimized SACs, achieving low overpotentials and high $CH_4$ selectivity. Cu–Al catalysts, optimized *via* ML and DFT, show improved faradaic efficiency and selectivity, with active learning refining the reaction conditions such as the temperature and pressure.[31] Thermocatalysis has benefited from AI platforms like Carbon Copilot (CARCO), which accelerated the discovery of SACs for $CO_2$ conversion, achieving high precision in catalyst design within weeks.[32] Mechanistic studies using ML and *ab initio* calculations, such as with CuPt/$TiO_2$ catalysts, reveal that interface design is crucial for stabilizing $CO_2$ intermediates, further guiding the rational design of SACs.[33]

While existing reviews[34–36] have extensively covered the preparation methods, characterization techniques, auxiliary agents, and catalyst supports for SACs, there is a notable paucity of discussions on the synergistic optimization of ML/DL/DFT approaches alongside experimental strategies in the design of SACs, the identification of optimal reaction conditions, and the fine-tuning of SACs preparation parameters. In this context, our review offers a comprehensive analysis of the preparation methods, characterization techniques, mechanistic insights, reaction kinetics, and the integration of ML predictions for SACs in $CO_2$RR. We emphasize the pivotal role of these approaches in optimizing the reaction pathways and enhancing the catalytic performance. Additionally, by employing machine learning to elucidate and validate the $CO_2$ reduction mechanisms, we aim to predict previously unexplored reduction pathways and intermediates, thereby providing a robust theoretical and technical foundation for the tailored production of advanced chemicals in industrial applications.

## 2 Single-atom catalysts: design, preparation, characterization and prediction

### 2.1 Formation and optimization of single-atom catalysts

The preparation of SACs involves dispersing isolated metal atoms onto a stable support to prevent aggregation into larger clusters or nanoparticles.[37] Single-atom dispersion requires strong metal–support interactions to prevent aggregation during synthesis or post-synthesis processes.[38,39] In wet-chemical methods, aggregation is inevitable unless the metal atoms or complexes strongly bind to the support. SACs consist of isolated metal atomic sites dispersed on a support, where metal atoms are not arranged in continuous lattice structures as in metal nanoparticles, nor embedded in the surface lattice of metal oxides or other non-oxide compounds. These active sites typically consist of the metal atom and its first coordination shell, composed of oxygen or other non-metallic atoms. The active sites interact with nearby surface structures, such as metal atoms and oxygen vacancies. These sites adsorb and activate reactant molecules, forming surface intermediates, and ultimately generate products. The structural complexity of SACs arises from the diversity of the ligand shells surrounding the dispersed metal atoms. These metal atoms are often located at defect sites on the support, such as step edges, corners, and voids. Although the metal atoms are isolated, their chemical and coordination environments vary significantly depending on their specific positions. This variation in ligand coordination induces different electronic perturbations in the metal atoms' valence orbitals, altering their electronic structure and ultimately affecting the catalytic performance (Fig. 1). Furthermore, the addition of two or more metal atoms to a single dispersed metal atom can form dimers or trimers, which often exhibit distinct an sometimes enhanced catalytic properties.

**Yizheng Li**

*Mr Yizheng LI is a PhD candidate, who is jointly affiliated with the Hong Kong Polytechnic University and the Eastern Institute of Technology (Ningbo) and advised by Prof. Zhangxing CHEN and Prof. Jinyue YAN. He received his M.Eng. and B.Eng. from China University of Petroleum-Beijing. His research interests primarily include interpretable artificial intelligence, machine learning, petroleum engineering, building energy management, clean energy production, energy policy, and sustainable engineering education.*

**Qidong Li**

*Mr Qidong Li earned his Master's degree in Electrical Engineering through a joint program between the University of British Columbia and the National Research Council Canada, after graduating with a Bachelor's degree in Process Equipment and Control Engineering from China University of Petroleum-Beijing. His research focuses on battery thermal management systems.*

$CO_2$RR has attracted considerable attention in recent years, especially in the fields of photocatalysis, electrocatalysis, and Fischer–Tropsch synthesis (FTS).[40,41] SACs have gained prominence due to their exceptional catalytic properties. When supported on materials such as carbon-based substrates, SACs can mimic the activation and reduction capabilities of homogeneous catalysts, facilitating $CO_2$ conversion into small organic molecules.[42] Despite their potential, challenges persist, including the strong C=O bond dissociation energy, competition with the hydrogen evolution reaction (HER), low product selectivity, and catalyst stability issues.[43] Recent advancements have focused on optimizing SACs to enhance $CO_2$ activation, tune electronic properties, and improve reaction pathways. For example, supporting SACs on nitrogen-doped carbon materials has been shown to significantly improve the $CO_2$RR efficiency by enhancing the charge transfer and stabilizing the key intermediates. Understanding and controlling the metal–support interaction is critical for improving the SACs performance, as it modulates the $CO_2$ binding energy and the formation of the desired products.

The use of a single-atom iron catalyst supported on carbon nitride has been demonstrated, where metal sites dispersed on a nitrogen-doped carbon matrix serve as active centers for the adsorption and activation of $CO_2$,[44] enabling its reduction to CO and hydrocarbons. Similarly, ultra-thin nitrogen-doped carbon nanosheets have been employed as supports for single-atom nickel catalysts, significantly enhancing the efficiency of $CO_2$RR. By integrating principles from homogeneous catalysis with quantum computational chemistry, these SACs have been engineered to mimic the $CO_2$ activation processes observed in homogeneous systems. Co-doping with carbon and nitrogen further boosts the catalytic efficiency by modifying the electronic environment of the SACs, optimizing the $CO_2$ adsorption, and facilitating the formation of reaction intermediates.

To further enhance the SACs catalytic performance, future development should focus on the following key aspects:

1. Optimization of metal–support interactions: tuning the interactions between metal active sites and the support is essential for improving the SACs performance. By modifying these interactions, the electronic structure of the metal atoms can be adjusted, thereby improving the $CO_2$ adsorption and facilitating the formation of reaction intermediates.

2. Synergistic effect of multi-metallic sites: incorporating two or more metal atoms into SACs can enhance its catalytic performance. This synergistic effect provides new avenues for SACs optimization.

3. Regulation of surface defects: introducing specific defects, such as oxygen vacancies or nitrogen doping, can effectively modulate the electronic environment of SACs, optimizing the catalytic pathways and enhancing the catalytic efficiency and selectivity.

4. Catalyst stability and reusability: improving the stability of SACs and preventing the loss or aggregation of metal atoms during prolonged reactions is essential for the industrial application of SACs.

### 2.2 Performance predictions by DFT and machine learning

**2.2.1 Structure-determined catalytic properties of single-atom catalysts.** The structure of SACs is crucial for their catalytic properties, particularly in $CO_2$RR. The geometric and electronic characteristics of SACs govern their activity, selectivity, and stability across different reaction conditions.[45] These properties depend on the active metal center,[46,47] its coordination environment, promoters, and support materials. Geometric features such as coordination number, bond lengths, and bond angles influence the distribution of active sites and the catalyst's interaction with reaction intermediates.[45–48] Catalysts

**Yuxuan Yi**

*Mr Yuxuan Yi is currently pursuing a Master's degree in Environmental Engineering at the National University of Singapore. His undergraduate research at Dalian University of Technology focused on photocatalysis. Presently, his research interests encompass seawater reverse osmosis and environmental data analytics.*

**Lifen Liu**

*Lifen Liu is currently a Full Professor in the School of Chemical Engineering, Marine and Life Science, Dalian University of Technology. She received her Bachelor, Master and Ph.D. degrees from DUT. She was a Visiting Scholar and Collaborator at the Sydney University, Australia from 1997–1999, a Research Associate at HKUST, HK, and a Senior Research Fellow at the Georgia Institute of Technology, USA (2010.10–2011.05). Her current and main scientific interests include environmental nanotechnology and pollution control engineering, specifically single-atom catalysts, functional electrode and fuel cell technologies for cost-effective processes. She has published more than 200 international peer-reviewed papers.*

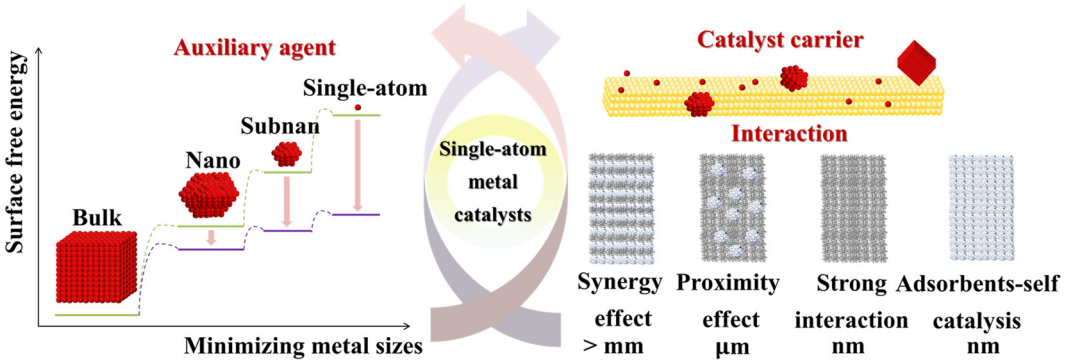


**Fig. 1** Effects of metal-size reduction on the surface free energy of auxiliary agents, and the interactions between auxiliary agents and catalyst supports in single-atom catalysts.



with unsaturated coordination sites often exhibit higher activity due to the better adsorption of the intermediates, and the bond structure affects $CO_2$ activation by modulating the electronic interactions between the catalyst and adsorbates.

The electronic structure of SACs is linked to bonding between the metal centers and reactants, with key factors such as the d-band center, electronegativity, and ionization energy playing a crucial role. The position of the d-band center controls electron transfer to adsorbed species, enhancing $CO_2$RR.[49] Electronegativity and ionization energy govern the catalyst's ability to donate or withdraw electrons, affecting interactions with $CO_2$ and products. Promoters such as alkali metals can further modify the electronic structure, adjusting the electron density and enhancing the adsorption of intermediates. The support material affects the metal dispersion, catalyst stability, and geometric configuration, influencing the electronic interactions and $CO_2$RR efficiency.

ML models are increasingly used to predict SAC performance in $CO_2$RR, leveraging high-dimensional data to uncover structure–activity relationships. Parameters such as the coordination number, bond length, d-band center, and electronegativity are key input features in these models. Computational methods like DFT predict the binding and adsorption energies, which are essential for understanding the $CO_2$RR mechanisms. These properties are fundamental in the rational design of optimized catalysts.[50]

Key structural features vary for different $CO_2$RR pathways, including photocatalysis, electrocatalysis, and thermocatalysis (Table 1). In photocatalysis, the band gap and electronic affinity govern light absorption and electron transfer efficiency. Electrocatalysis emphasizes charge transfer and the d-band center for efficient electron flow at the electrode surface. In thermocatalysis, geometric descriptors like the coordination number and bond lengths are critical for the reaction rate and product distribution, particularly at high temperatures.

**2.2.2 Explanation and validation of the reaction mechanism.** The use of SACs for $CO_2$RR to produce value-added chemicals, through photocatalysis,[51] electrocatalysis,[27] and thermocatalysis,[52] requires an in-depth understanding of the underlying reaction mechanisms. Recent developments in ML, integrated with DFT, have become pivotal tools for unraveling these mechanisms by predicting the reaction dynamics, energy profiles, and intermediates, thus advancing the design of efficient catalysts.

Machine learning models, particularly those integrated with DFT calculations, have shown significant potential in predicting the electronic structure and energetics of SACs. For instance, the first-coordination sphere–support interaction (FCSSI) has emerged as a key descriptor for regulating the catalyst performance in $CO_2$RR. ML models, such as extreme gradient boosting regression (XGBR), utilize DFT-derived data to predict limiting potentials (UL), which directly influence reaction pathways and selectivity toward specific products.[53] Moreover, ML has proven effective in identifying intermediate species and elucidating reaction pathways. For example, the use of ML models to predict product selectivity in SACs supported on modified graphene (*e.g.*, $MoO_4$ on H-doped graphene and $FeO_4$ on N,O-doped graphene) demonstrated the ability to distinguish between products like formate and CO.[54] This highlights the potential of ML to identify SACs that minimize side reactions, such as HER,[55] and favor target products such as formic acid or CO. In addition to predicting known pathways, ML models can uncover previously unobserved reaction mechanisms. For example, the prediction of new C–C coupling processes in graphdiyne-based SACs for $C_3$ product formation offers new possibilities for $CO_2$RR, potentially enhancing the overall $CO_2$ conversion efficiency.[56] These models provide an integrated framework to validate existing hypotheses and predict novel catalytic routes, which is critical for developing more selective and efficient $CO_2$RR catalysts.

The application of graph neural networks (GNNs) and transformer-based models, such as CatBERTa, has further strengthened the predictive capabilities of ML models. These hybrid models can predict adsorption energies by utilizing spatial coordinates and textual representations of catalytic systems, thus allowing for the discovery of unknown intermediates and reaction pathways.[57] Additionally, ML models can identify optimal reaction conditions, such as metal centers (Mn, Co, Ru, Os) and support interactions, which are crucial for product

 

Table 1 Summary of the descriptors for machine learning models of single-atom catalysts in $CO_2$ reduction reactions *via* photocatalysis, electrocatalysis, and thermocatalysis

| Descriptors | Photocatalysis | Electrocatalysis | Thermocatalysis |
|---|---|---|---|
| **Structural and geometrical properties** | | | |
| Bond lengths | ✓ | ✓ | ✓ |
| Bond angles | ✓ | ✓ | ✓ |
| Atomic radius | ✓ | ✓ | ✓ |
| Coordination numbers | ✓ | ✓ | ✓ |
| Atomic positions (one-hot encoding) | ✓ | ✓ | ✓ |
| Number of specific element atoms | ✓ | ✓ | ✓ |
| Surface hollow, bridge, and top sites | ✓ | ✓ | ✓ |
| **Chemical and elemental properties** | | | |
| Electronegativity | ✓ | ✓ | ✓ |
| Ionization energy | ✓ | ✓ | ✓ |
| Atomic mass | ✓ | ✓ | ✓ |
| d-electron count | ✓ | ✓ | ✓ |
| d-band center | ✓ | ✓ | ✓ |
| Valence electron number | ✓ | ✓ | ✓ |
| Electron affinity | ✓ | ✓ | ✓ |
| **Physics-informed descriptors** | | | |
| SOAP (smooth overlap of atomic positions) | ✓ | ✓ | ✓ |
| MBTR (many-body tensor representation) | ✓ | ✓ | ✓ |
| ACSF (atom-centered symmetry functions) | ✓ | ✓ | ✓ |
| **Synthesis and experimental parameters** | | | |
| Calcination temperature (°C) | | ✓ | ✓ |
| Calcination time (h) | | ✓ | ✓ |
| Reduction temperature (°C) | | ✓ | ✓ |
| Reduction time (hours) | | ✓ | ✓ |
| Reaction temperature (°C) | ✓ | ✓ | ✓ |
| Reaction pressure (MPa) | ✓ | ✓ | ✓ |
| GHSV | ✓ | ✓ | ✓ |
| Time on stream (h) | ✓ | ✓ | ✓ |
| **Experimental data and metrics** | | | |
| Tafel slope ($\eta$) | | ✓ | |
| Band gap (eV) | ✓ | | |
| Catalyst per volume (mg $mL^{-1}$) | ✓ | | |
| Sacrificial agent | ✓ | | |

selectivity, as seen in the case of $CH_4$ production.[58] By integrating ML with computational studies, the exploration of $CO_2$RR mechanisms becomes more systematic and accurate. This approach not only allows for the identification of new intermediates and reaction steps, but also enables experimental validation, which accelerates the discovery of high-performance SACs. The synergy between ML predictions and experimental data fosters an iterative process that refines reaction mechanism models, facilitating the rational design of SACs for efficient $CO_2$RR.

ML-based methods, when coupled with quantum-level simulations, offer valuable insights into $CO_2$RR mechanisms on SACs. These approaches facilitate the prediction of intermediates, reaction pathways, and optimal conditions, leading to the design of SACs with tailored properties for enhanced $CO_2$RR performance.

**2.2.3 Designing single-atom catalysts and optimizing reaction conditions.** The design and optimization of SACs for $CO_2$RR rely on predicting catalytic properties, which depend on the catalyst structure, support material, and reaction conditions. ML models are highly effective in predicting the impact of the synthesis strategies on catalyst performance by using descriptors, such as the coordination number, d-band center, and local chemical environments. These models aid in selecting the most efficient SAC compositions and predicting the adsorption energies of $CO_2$RR intermediates, thereby guiding the design of SACs for specific products, such as CO or formic acid.[59] Additionally, ML assists in optimizing reaction conditions (*e.g.*, temperature, pressure, and electrolyte composition), which are crucial for enhancing the catalyst stability, selectivity, and efficiency. Through DL and active learning, ML can identify the reaction conditions that suppress side reactions, such as hydrogen evolution.[60]

Active ML methods, including reinforcement and self-supervised learning, enable models to autonomously search for optimal SAC structures and reaction conditions. These models iteratively refine predictions through continuous feedback from experimental data, accelerating the discovery of high-performance SACs. Moreover, ML facilitates the design of catalyst supports and surface modifications by considering local coordination environments and the electronic effects induced by dopants.[54] In practical applications, ML has already contributed to the discovery of SACs such as Zn-$NP_3$ and Sn-$P_4$, which exhibit promising $CO_2$RR activity and selectivity.[60] By predicting the optimal catalyst structures and conditions before synthesis, these models minimize trial-and-error processes and accelerate the development of efficient SACs for $CO_2$RR. Furthermore, ML-driven frameworks enable

the high-throughput screening of catalyst materials and reaction parameters, expediting the discovery of novel SACs. The iterative refinement of SAC structures and reaction conditions continuously enhances the catalyst performance and $CO_2$ utilization strategies.

In summary, integrating ML with SAC design and optimization offers a transformative approach to developing high-performance catalysts. By predicting the optimal catalyst structures and reaction conditions, ML accelerates the discovery and optimization of SACs for more efficient $CO_2$RR.

**2.2.4 Mutual verification framework integrating DFT and machine learning.** DFT plays a pivotal role in elucidating the electronic structure, adsorption behavior, and reaction mechanisms at active sites, effectively complementing experimental studies. With its high accuracy, DFT facilitates the interpretation of experimental observations and the prediction of catalytic performance, effectively bridging experimental data with theoretical models. These calculations are indispensable for optimizing the design of SACs and refining catalytic pathways. However, the high computational cost of DFT poses challenges, particularly when modeling large or complex systems.

To address these computational limitations, various ML models, including Random Forest (RF), Support Vector Machines (SVM), Neural Networks (NN), and Graph Neural Networks (GNNs), have been employed to predict the catalytic performance of SACs and gain insights into their underlying mechanisms. These models utilize the structural and electronic properties of catalysts to predict the catalytic activity, stability, selectivity, and key reaction parameters such as activation energy and charge transfer.

From a mechanistic perspective, Zhu *et al.*[61] identified eight key descriptors that characterize the electronic and structural properties of catalysts: $N_d$ (the number of d-shell valence electrons of metal atoms), which influences reactivity; EA (electron affinity), representing the metal's ability to accept electrons; CT (charge transfer from metal-zeolites to intermediates), quantifying electron redistribution during the catalytic step; $H_c$ (hydrogen count in carbon atoms) and $H_s$ (hydrogen in $H_2O$, $CH_3OH$, $CH_4$), which influence the reactant activation; $N_c$ (coordination number of carbon to metal), capturing the interaction strength between the carbon-based intermediates and the metal; $P_s$ (number of proton/electron transfers), offering insights into the proton or electron transfer mechanisms; and $N_{HB}$ (hydrogen bonds), which stabilize the reaction intermediates.

To predict CT (e)—the charge transfer between the metal-zeolites and intermediates—ML models are trained using three key features: $C$ (coordination number for intermediate to metal), $N_o$ (coordination number for oxygen to metal), and NI (number of atoms in intermediates). These features capture the strength of the interaction between intermediates and the metal, the interaction of oxygen-containing species with the metal, and the complexity of the intermediates. By analyzing the relationships between these features and charge transfer, ML models help identify active sites and understand the critical electronic redistributions necessary for catalytic activity (Fig. 2).

Once trained, ML models can predict key DFT-derived quantities, such as CT (e), activation barriers, and intermediate energies, at a significantly reduced computational cost. This accelerates the screening of catalysts and intermediates, allowing DFT calculations to focus on the most promising candidates. Additionally, ML enables efficient exploration of complex parameter spaces, uncovering insights into the reaction mechanisms that DFT alone might not fully resolve.

From a mechanistic perspective, ML provides deeper insights into catalytic processes by identifying key descriptors and elucidating their influence on reactivity. It offers a fundamental understanding of how electronic structures drive charge transfer and how intermediate coordination impacts catalytic efficiency. The integration of ML with DFT and experimental data accelerates SACs discovery and optimization, providing a powerful framework for designing next-generation catalytic materials with tailored properties.

### 2.3 Efficient and innovative methods for the preparation of single-atom catalysts

The preparation methods for SACs impact their performance in $CO_2$ reduction, with each method offering distinct advantages and limitations (Fig. 3). Co-precipitation is cost-effective and scalable, yielding SACs with high surface area and catalytic activity.[62] However, high metal loading can cause aggregation, reducing catalyst efficiency. It is suitable for large-scale production, but struggles with metal dispersion at high loadings.[63]

Ion exchange enables precise metal deposition, increasing active site density and surface area,[64,65] but suffers from high reagent consumption and catalyst instability[66] due to site degradation.[67] Chemical vapor deposition (CVD) and atomic layer deposition (ALD) achieve atomic-level metal dispersion, yet remain cost-intensive and complex, limiting their scalability. The sol–gel method, though solvent-free with good dispersion, risks metal aggregation at high temperatures. Electrodeposition, often following substrate cleaning and electropolishing, facilitates nanostructure formation, while spin-coating efficiently deposits functional layers like perovskites, followed by annealing. Hydrothermal synthesis grows metal oxide nanowires, and photolithography with etching fabricates precise substrate patterns.[68]

For large-scale applications, co-precipitation offers cost efficiency and scalability, whereas CVD and ALD provide superior atomic precision but face economic and scalability constraints. The optimal method depends on balancing the cost, precision, and industrial feasibility.

### 2.4 Comparison in the characterization of single-atom catalysts

Accurate characterization is crucial for understanding the structure–property relationships of SACs, which exhibit unique catalytic behaviors due to their atomically dispersed active sites. The complexity of SACs, including their coordination environment, electronic structure, and metal–support interactions, requires the use of complementary techniques that

 

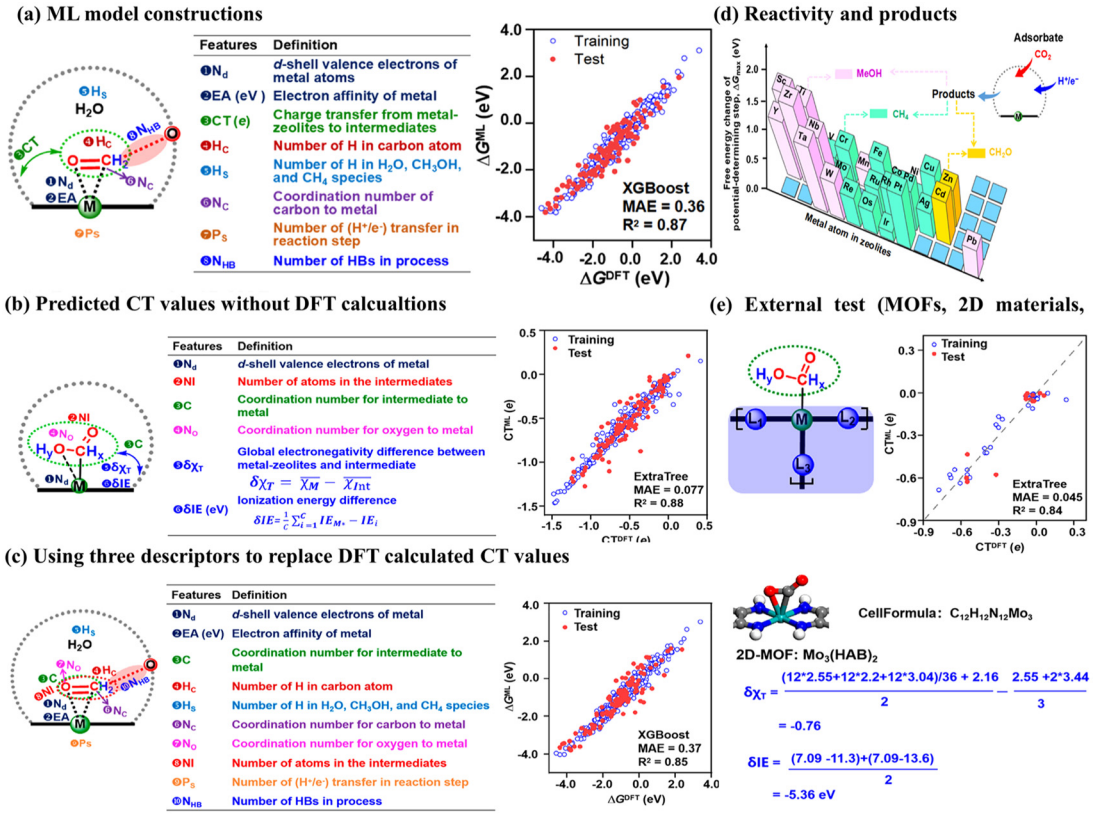


**Fig. 2** Application of DFT and machine learning/deep learning in predicting reaction pathways (a) Machine learning model with eight features, and the ability the XGBoost algorithm in predicting the free energy change in $CO_2$ reduction process, (b) Machine learning model with six features for CT prediction on metal-zeolites, (c) 10-feature scheme, using three additional descriptors to replace the CT values, for free energy change prediction in the $CO_2$ reduction process using XGBoost, (d) flow chart of reactivity and product calculation of $CO_2$ reduction reactions on 26 metal-zeolites, (e) external test in the $CO_2$ reduction process using ExtraTree. Reproduced from ref. 61, with permission of ACS Catalyst, copyright 2022.

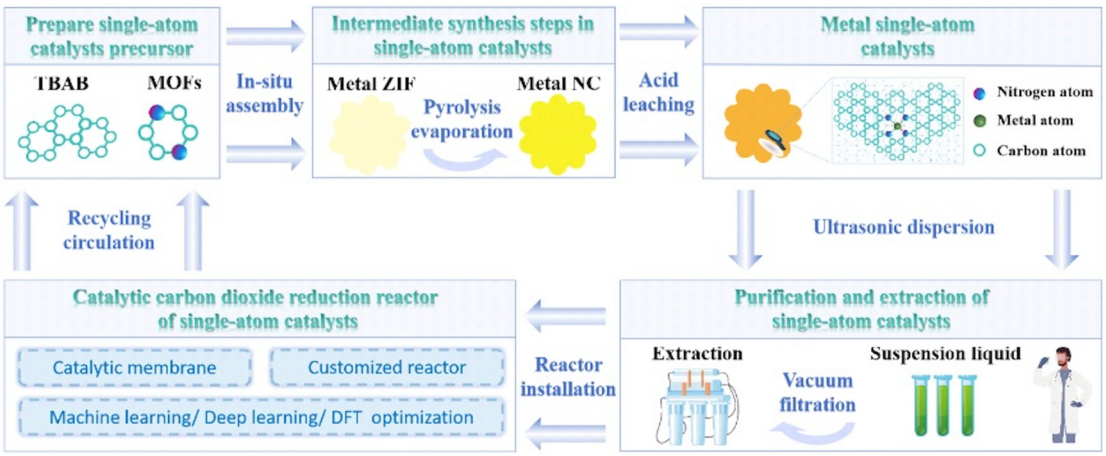


**Fig. 3** Synthesis, purification, and application of single-atom catalysts for $CO_2$ reduction: from precursor preparation to catalytic reactor implementation.

each address specific aspects of their structure and performance.

Microscopic methods, such as transmission electron microscopy (TEM) and scanning transmission electron microscopy (STEM) combined with energy-dispersive X-ray spectroscopy (EDS), provide spatial insights into the dispersion and localization of single atoms. TEM reveals the distribution of active sites, while STEM-EDS achieves atomic-scale resolu-

tion, providing detailed insights into the elemental composition and structural features. Spectroscopic techniques, including X-ray absorption fine structure (XAFS) and X-ray photoelectron spectroscopy (XPS), play a crucial role in probing the local coordination environment, oxidation state, and chemical bonding of single atoms. These methods reveal the critical interactions between the active sites and the support, while also characterizing the surface's elemental composition and chemical states.

*In situ* techniques, such as Fourier transform infrared spectroscopy (FTIR) and Raman spectroscopy, allow for real-time monitoring of active sites and surface chemical environments during reactions. FTIR monitors the adsorption behavior and vibrational modes of reaction intermediates, while Raman spectroscopy tracks dynamic changes in catalytic sites under reaction conditions, elucidating the reaction mechanisms. Thermal characterization methods, such as temperature-programmed reduction (TPR) and thermogravimetric analysis (TGA), assess metal–support interaction strength, reducibility, and thermal stability, all of which are essential for evaluating the catalyst durability under operational conditions.

The integration of these techniques offers a comprehensive understanding of SACs, connecting their atomic structure, electronic properties, and reaction mechanisms to the catalytic performance and selectivity. This holistic approach not only advances fundamental knowledge, but also informs the rational design of next-generation catalysts for $CO_2$ hydrogenation and other critical reactions.

# 3 Photocatalytic $CO_2$ reduction

## 3.1 Mechanism of photocatalytic reduction

The photocatalytic reduction of $CO_2$ with $H_2$ utilizes light energy, typically from ultraviolet or visible light, to drive the reaction, converting $CO_2$ and $H_2$ into valuable products such as methane, methanol, and other organic compounds. This process involves several critical steps. First, photon absorption occurs when the semiconductor catalyst absorbs light, exciting electrons from the valence band to the conduction band, thereby generating electron–hole pairs ($e^-/H^+$). The electrons and holes are then separated and migrate within the catalyst's conduction and valence bands, with electrons ($e^-$) participating in the $CO_2$RR, while holes ($H^+$) are involved in the oxidation of $H_2$. During $CO_2$RR, the electrons reduce $CO_2$ into products such as carbon monoxide, methanol, or methane, depending on the catalyst and reaction conditions. This reaction proceeds through $e^-$ and $H^+$ transfer, with different intermediates forming based on the targeted product. The oxidation process involves $H^+$ at the catalyst surface, which oxidize $H_2$, generating $H^+$ that provide the protons necessary for $CO_2$RR. These key steps are crucial for optimizing the catalyst performance and guiding the development of efficient photocatalysts for $CO_2$ hydrogenation (Table 2).

In photocatalytic $CO_2$ hydrogenation, the use of SACs is particularly effective. SACs, with their atomic-level dispersion on supports, create well-defined active sites that facilitate efficient electron and proton transfer, thereby optimizing the reduction steps. These catalysts enhance the reaction rates, selectivity, and stability by minimizing energy barriers, stabilizing reaction intermediates, and promoting specific electron transfer processes. The preparation of SACs—including metal choice, support material, and synthesis method—significantly influences their catalytic performance. By fine-tuning the electronic properties of metal atoms and their interaction with the support, SACs can be optimized to enhance $CO_2$ activation, improve product selectivity, and boost the overall efficiency of the photocatalytic reduction process (Fig. 4).

Inspired by photosynthesis, photocatalysis leverages light-driven redox reactions for $CO_2$ fixation. In this process, photogenerated charge carriers are separated in the semiconductor[69] and transferred to the catalyst surface, where they react with adsorbed $CO_2$. This results in the conversion of $CO_2$ into valuable organic compounds such as formic acid, CO, alcohols, and hydrocarbons.[70] Compared to traditional $CO_2$ purification methods, photocatalysis offers advantages such as mild reaction conditions, low energy consumption, and minimal environmental impact, positioning it as a promising technology for sustainable $CO_2$ utilization and carbon management.[71]

## 3.2 Reaction kinetics of photocatalytic reduction

The reaction kinetics of photocatalytic $CO_2$RR, particularly when catalyzed by SACs, begins with photon absorption, which excites electrons and generates active sites on the cata-

**Table 2** Equilibrium potential ($E_{eq}$ *vs.* RHE) and reaction enthalpy ($\Delta H$) for the reduction of $CO_2$ to different products

| Product | $CO_2$ reduction pathways | $E_{eq}$ (V) | $\Delta H$ (kJ mol$^{-1}$) |
|---|---|---|---|
| CO | $CO_2 + 2e^- + 2H^+ \rightarrow CO + H_2O$ | −0.10 | −41.2 |
| $CH_4$ | $CO_2 + 8e^- + 8H^+ \rightarrow CH_4 + 2H_2O$ | 0.17 | −253.0 |
| $C_2H_6$ | $2CO_2 + 14e^- + 14H^+ \rightarrow C_2H_6 + 4H_2O$ | 0.14 | 264.3 |
| $C_3H_8$ | $3CO_2 + 20e^- + 20H^+ \rightarrow C_3H_8 + 6H_2O$ | 0.09 | 374.2 |
| $C_2H_4$ | $2CO_2 + 12e^- + 12H^+ \rightarrow C_2H_4 + 4H_2O$ | 0.08 | 127.8 |
| $CH_3OH$ | $CO_2 + 6e^- + 6H^+ \rightarrow CH_3OH + H_2O$ | 0.03 | −131.0 |
| $C_2H_5OH$ | $2CO_2 + 12e^- + 12H^+ \rightarrow C_2H_5OH + 3H_2O$ | 0.09 | 216.1 |
| $C_3H_7OH$ | $3CO_2 + 18e^- + 18H^+ \rightarrow C_3H_7OH + 5H_2O$ | 0.1 | 331.2 |
| $CH_3CHO$ | $2CO_2 + 10e^- + 10H^+ \rightarrow CH_3CHO + 3H_2O$ | 0.06 | 130.1 |
| HCOOH | $CO_2 + 2e^- + 2H^+ \rightarrow HCOOH$ | −0.12 | −31.2 |
| $CH_3COOH$ | $2CO_2 + 10e^- + 10H^+ \rightarrow CH_3COOH + 2H_2O$ | 0.11 | 122.1 |

 

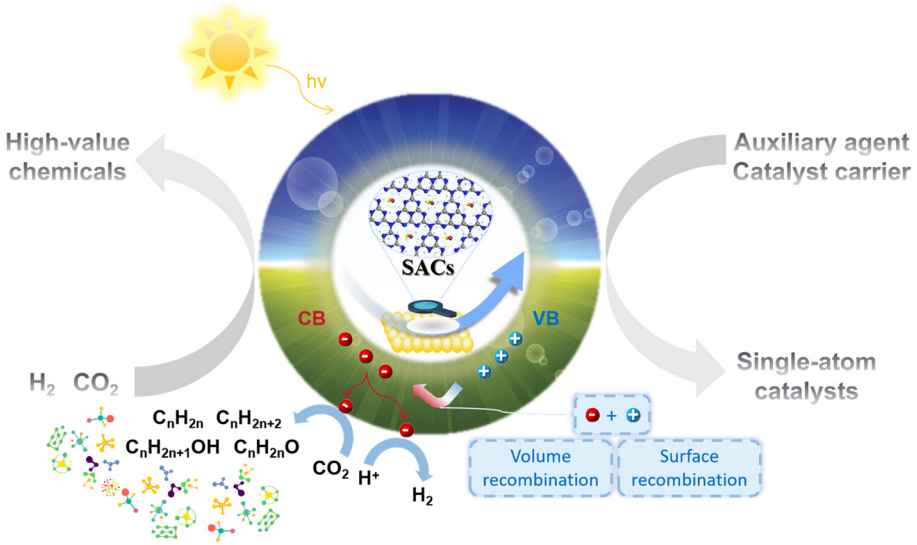


**Fig. 4** Engineering single-atom catalysts for efficient photocatalytic $CO_2$ reduction: modulation of the electron pair alignment and recombination dynamics using auxiliary agents and catalyst supports to enhance the catalyst stability.

lyst surface. The efficiency of this process is largely influenced by the metal's ability to facilitate electron transfer and the support material's role in stabilizing the excited states. Early research on photocatalytic $CO_2$RR dates back to the 1970s, initially focusing on semiconductor materials for water splitting applications. In the 1980s, research shifted towards using solar energy to drive $CO_2$RR into organic chemicals, with early studies concentrating on methane and carbon monoxide production. Initial reaction models were oversimplified, typically assuming surface adsorption and electron transfer as the primary steps. However, with advancements in the catalyst materials and reaction conditions, the kinetics of the process became increasingly complex, involving multiple steps, various intermediates, and charge carrier participation.

As catalyst materials diversified, selectivity and product distribution in photocatalytic $CO_2$RR emerged as critical research themes. Different catalysts not only affect the separation efficiency of electron–hole pairs, but also play a decisive role in the formation pathways of intermediates, thus determining the final product. The reaction kinetics of photocatalysis involve several complex stages, including catalyst excitation, electron–hole pair separation and migration, and the formation and transformation of intermediates.

Enhancements in reaction kinetics are often achieved through orbital coupling between metal atoms and adjacent ligands, especially in bimetallic sites. For instance, Pt–Ru dimers on g-$C_3N_4$ demonstrate significantly improved catalytic performance for $CO_2$RR and HER by weakening the binding strength with intermediates and adjusting the orbital energy levels.[72] This strategy allows for more efficient catalytic processes by optimizing the interaction between the catalyst and the reaction intermediates.

$$r_{PC} = k_{PC} \cdot I_{light}^{n_{PC}} \cdot (C_{CO_2})^{a_{PC}} \cdot (C_{H_2})^{b_{PC}}$$

The rate of a photocatalytic reaction ($r_{PC}$) is generally linearly dependent on the light intensity ($I_{light}$). However, under high light conditions, the reaction rate may become limited by the catalyst's electron carrier capacity, resulting in kinetic saturation. The rate is also influenced by the concentrations of $CO_2$ ($C_{CO_2}$) and $H_2$ ($C_{H_2}$), as well as by the surface adsorption characteristics of the catalyst, illumination conditions, and reactant concentrations (*e.g.*, $n_{PC}$, $a_{PC}$, $b_{PC}$). Moreover, the lifetime of the photogenerated electrons and the efficiency of the charge carrier separation are critical factors that impact the overall reaction efficiency. The separation efficiency of charge carriers is closely related to the catalyst surface structure and the light intensity. If photogenerated electrons recombine with holes on the catalyst surface, the reaction efficiency will be significantly reduced. Therefore, optimizing the charge carrier migration and separation efficiency is crucial for improving the performance of photocatalytic $CO_2$ reduction.

### 3.3 Photocatalytic reduction of $CO_2$ using single-atom catalysts

**3.3.1 Mechanisms of auxiliary agents in photocatalysts.** The photocatalytic reduction of $CO_2$, first explored by Fujishima *et al.*[73] in 1972 using $TiO_2$ for water splitting and later advanced by Halmann[74] in 1978 for $CO_2$ conversion to formic acid and methanol, has attracted substantial interest due to its potential in sustainable $CO_2$ utilization. This process offers several advantages, including mild reaction conditions (ambient temperature and pressure), the use of renewable solar energy, and an environmentally friendly approach.[75] However, the efficiency of photocatalytic $CO_2$RR is still hindered by challenges such as inefficient charge separation,[76] low energy transfer efficiency, and limited $CO_2$ adsorption and activation on catalyst surfaces. Addressing these limitations is crucial for advancing practical applications.[77,78]

Optimizing $CO_2$ adsorption and activation on the catalyst surface is key to improving the photocatalytic performance. However, a detailed understanding of surface site dynamics is still lacking. Feng *et al.*[79] introduced an innovative strategy by constructing Mn single-atom sites on $TiO_2$ nanostructures, which modified the local coordination environment, enhancing $CO_2$ adsorption and the localization of photogenerated electrons, thus improving the catalytic efficiency. Similarly, Zhang *et al.*[80] developed a dual-site system combining Au/Co double-monoatom-supported CdS for $CO_2$RR. In this system, Co sites promote $CO_2$ adsorption and reduction, while Au sites facilitate the collection of photogenerated electrons, selectively producing CO and $CH_4$ with 82% selectivity. This design underscores the importance of effectively distributing photogenerated charges across different single-atom sites to enhance the photocatalytic selectivity.

Auxiliary agents play a vital role in optimizing SACs for photocatalytic $CO_2$RR by modulating their electronic structures, stabilizing active sites, and facilitating charge transfer. Strategies such as defect engineering, heteroatom doping, and co-catalyst integration significantly influence reaction pathways, improving the catalytic activity and product selectivity.[81–83] One effective approach involves introducing oxygen vacancies or structural distortions in the catalyst support to enhance the $CO_2$ adsorption and charge separation. For instance, in Pd-SA/$TiO_2$, oxygen vacancies created under a hydrogen-rich atmosphere serve as strong anchoring sites for Pd single atoms, preventing agglomeration and tuning their electronic structure. This modification increases the CO selectivity to 92.51% and catalytic activity to 56.84 μmol $g^{-1}$ $h^{-1}$ by facilitating charge transfer and minimizing electron–hole recombination.[84]

Heteroatom doping further refines the electronic properties of SACs by modifying charge distribution at the active sites. Doping with elements such as nitrogen, sulfur, or phosphorus stabilizes the reaction intermediates and enhances $CO_2$ activation. In Cu-based SACs, nitrogen-doped carbon supports strengthen metal–support interactions, promoting C–C coupling and enabling selective $C_{2+}$ product formation. The dopant atoms shift the d-band center of the Cu sites, reducing the activation energy barriers and optimizing multi-electron transfer processes.[85]

Co-catalyst incorporation provides another effective strategy for improving SACs performance by introducing additional charge transfer pathways or cooperative catalytic mechanisms.[86] Overall, the integration of defect engineering, heteroatom doping, and co-catalysts significantly enhances SACs performance in photocatalytic $CO_2$RR. These strategies collectively improve charge transfer, stabilize reaction intermediates, and suppress recombination losses, leading to higher catalytic efficiency and selectivity.

**3.3.2 Supports for photocatalysts.** The inherent chemical inertness of $CO_2$, combined with weak adsorption and high activation barriers, poses significant challenges for efficient $CO_2$RR, especially at low concentrations. Additionally, competitive HER further hinders progress in this area. To overcome these obstacles, Lyu *et al.*[87] designed oxygen-deficient $Co_3O_4$ hollow nanoparticles supported on a macroporous N-doped carbon framework. The introduction of oxygen vacancies disrupted the Co–O–Co symmetry, enhancing $CO_2$ adsorption and activation, while the macroporous structure increased active site availability and facilitated the transport of photogenerated electrons. This work underscores the importance of active site symmetry modulation for improving catalytic performance in low-concentration $CO_2$RR.

MOFs have attracted considerable interest for their ability to modulate electron transport in photocatalysis, owing to their tunable porosity, high surface area, and the potential to tailor active sites. Porphyrins and their derivatives, known for their excellent photosensitivity, can create conductive pathways through their stacked units. The incorporation of metals further enhances electron transport, although precise control of these pathways remains a challenge. Huang *et al.*[88] employed a thermal-induced strategy, using thorium ions as unstable coordination nodes in porphyrin-based MOFs to control electron transport, thereby improving carrier separation and enhancing photocatalytic efficiency. This study provides valuable insights into carrier dynamics within photocatalytic systems. MOFs provide high surface area, tunable porosity, and defined coordination sites, ensuring uniform metal dispersion and electronic modulation. Their confinement effect prevents metal aggregation, while enhancing $CO_2$ activation. MOF-derived carbons retain structural integrity and improve conductivity, facilitating charge transfer and reaction kinetics.

Recent developments in SACs have demonstrated their potential for $CO_2$RR, driven by their unique electronic properties, high dispersion, and enhanced catalytic activity through defect engineering. SACs offer additional active sites at the atomic scale, which significantly enhance catalytic performance. Cheng *et al.*[89] utilized the large surface area and planar conjugate structure of g-$C_3N_4$ to anchor Ni single atoms through a self-limiting method.[90] This approach not only stabilized the Ni single atoms, but also promoted efficient $CO_2$ adsorption and electron transfer from g-$C_3N_4$ to Ni *via* Ni–N coordination, resulting in a $CO_2$ conversion rate that is 7.8 times higher than that of pure g-$C_3N_4$ under visible light. This highlights the critical role of tuning active sites for improving $CO_2$RR efficiency.[91]

Zhang *et al.*[92] developed Co-SA@SP by anchoring single-atom cobalt on commercial superconducting carbon black. The Co–$N_4$ coordination sites in this material reduced the $CO^{\bullet}$ desorption energy barrier, enhancing the catalytic reactivity, CO selectivity (84.2%), and stability under UV light. The suppression of HER further promoted $CO_2$RR, demonstrating the potential of SACs to inhibit competitive reactions and enhance selectivity. This simple and cost-effective catalyst offers a promising pathway for scalable photocatalytic $CO_2$RR in industrial applications. Catalyst carriers critically influence SACs' photocatalytic $CO_2$RR by modulating the electronic structure, charge transfer, and active site stability. The carrier dictates metal–support interactions, adsorption strength, and reaction selectivity.

 

Semiconductor supports with oxygen vacancies effectively anchor single metal atoms, preventing aggregation while tuning their electronic environment. In Pd-SA/$TiO_2$, oxygen vacancies enhance metal–support interactions, optimizing Pd's oxidation state and $CO_2$ activation. This defect engineering improves the charge separation and suppresses recombination, boosting the catalytic efficiency.[84]

Carbon-based supports, such as graphene, CNTs, and nitrogen-doped carbon (N–C), offer high conductivity and π-conjugation networks that enhance charge transport. In Cu-SACs, N–C stabilizes Cu atoms, improving C–C coupling and favoring $C_{2+}$ products. Strong metal–support interactions (SMSI) optimize Cu's electronic state, lowering activation barriers and increasing the $CO_2$ conversion selectivity.[85] Hybrid architectures incorporating plasmonic nanostructures or co-catalysts further enhance the SACs performance. Plasmonic-metal-SACs hybrids use localized surface plasmon resonance (LSPR) to extend the carrier lifetimes and improve charge transfer, lowering the activation barriers. Co-catalyst integration facilitates charge separation and directional electron flow, optimizing the reaction selectivity.[86]

In summary, defect engineering, conductivity tuning, and confinement effects are key to improving the SACs stability and reactivity. Future research should focus on optimizing the metal–support interactions and charge transfer pathways to enhance SAC-based $CO_2$RR.

**3.3.3 Perovskite-structured photocatalysts.** In photocatalytic $CO_2$RR, perovskite-based SACs have garnered considerable attention due to their unique structural and electronic properties, which enhance their catalytic performance. Perovskite materials, with their distinctive crystal structures, offer multiple advantages in the context of SACs for $CO_2$RR.

The perovskite structure, characterized by a corner-sharing octahedral arrangement of metal cations and halide anions, provides a versatile platform for modulating the electronic properties, optimizing the charge carrier dynamics, and facilitating enhanced photocatalytic activity. In $Cs_3Sb_{0.5}Bi_{1.5}Cl_4Br_5$ perovskite catalysts, the formation of a built-in electric field (IEF) within heterojunctions facilitates efficient electron–hole separation, a key factor in improving the photocatalytic $CO_2$RR efficiency. The coupling of these materials with other catalysts, such as Bi-BTC frameworks, has shown that the synergistic effects between the two components can significantly boost photocatalytic performance, leading to high CO and $CH_4$ yields.[93]

In addition, engineering the electronic structure of perovskites through doping or phase transition can further enhance their catalytic properties. For example, doping perovskite structures with metal ions or using phase transitions to generate piezoelectricity can increase the adsorption capacity for $CO_2$ and reduce the energy barrier for its conversion.[94] The piezoelectric effect, induced by phase transition under external stimuli, can produce a polarized electric field that accelerates $CO_2$ activation, contributing to improved catalytic efficiency. In the case of $Cs_3Bi_2Br_9$-based perovskites, the introduction of Cu atoms into the perovskite lattice has been shown to promote charge separation and enhance the electronic structure of the material, which further lowers the energy barriers for $CO_2$RR. The atomically dispersed Cu acts as a critical site for charge transfer, improving the selectivity for CO production while maintaining stability over multiple cycles.[95]

The engineering of heterojunctions by combining perovskites with other semiconductors, such as $Co_3O_4$, has proven highly effective for promoting efficient charge separation. The formation of built-in electric fields at the heterojunction interface enhances the photocatalytic $CO_2$RR performance, with Na-ion incorporation further strengthening these electric fields to boost $CO_2$ adsorption and activation.[96] Thus, perovskite SACs possess unique properties, such as their tunable band structures, efficient charge separation, and enhanced $CO_2$ adsorption, all of which play crucial roles in improving the directional selectivity of photocatalytic $CO_2$RR.[97] These structural features, coupled with innovative doping strategies and heterojunction formation, position perovskite-based SACs as promising candidates for the efficient conversion of $CO_2$ into valuable chemicals (Fig. 5).

# 4 Electrocatalytic $CO_2$ reduction

## 4.1 Mechanism of electrocatalytic reduction

$CO_2$RR converts electrical energy into chemical energy, producing valuable small molecules *via* electrochemical reduction.[92] However, in aqueous systems, the HER often competes with $CO_2$RR, significantly reducing selectivity and efficiency. To address this, the development of highly efficient electrocatalysts with high activity, selectivity, and stability is crucial for advancing $CO_2$RR technology. SACs have emerged as promising candidates due to their well-defined active sites, maximizing atom utilization. The performance of SACs is primarily determined by the electronic structure and coordination environment of the single metal atoms, which can effectively modulate $CO_2$ adsorption, activation, and reduction. SACs promote the reduction process by facilitating the formation of key intermediates such as $^*CO_2$, $^*COOH$, and $^*CHO$ through unique reaction pathways, while minimizing HER by optimizing the binding energies of hydrogen and $CO_2$ intermediates. The enhanced selectivity and efficiency of SACs arise from the atomic-level control over the reaction mechanisms, enabling precise tuning of the product distribution. Ongoing efforts to improve SACs for $CO_2$RR have focused on stabilizing the metal sites, increasing conductivity, and optimizing the local electronic environment to achieve scalable, practical performance.

$CO_2$RR is a complex multi-electron, multi-proton process where intermediates like $^*CO$ are crucial for $C_2$ product formation. Strong interactions between $^*CO$ and metal catalysts (*e.g.*, Pt, Fe, Ni) can poison the active sites, favoring HER and diminishing the $CO_2$RR efficiency.[98] On the other hand, metals with weak $^*CO$ binding (*e.g.*, Au, Ag, Zn) facilitate $^*CO$ desorption, which prevents efficient C–C coupling and results in CO as the final product.[99] However, metals with moderate $^*CO$ binding strengths, such as Cu, Ni, Co, and Zn, are among

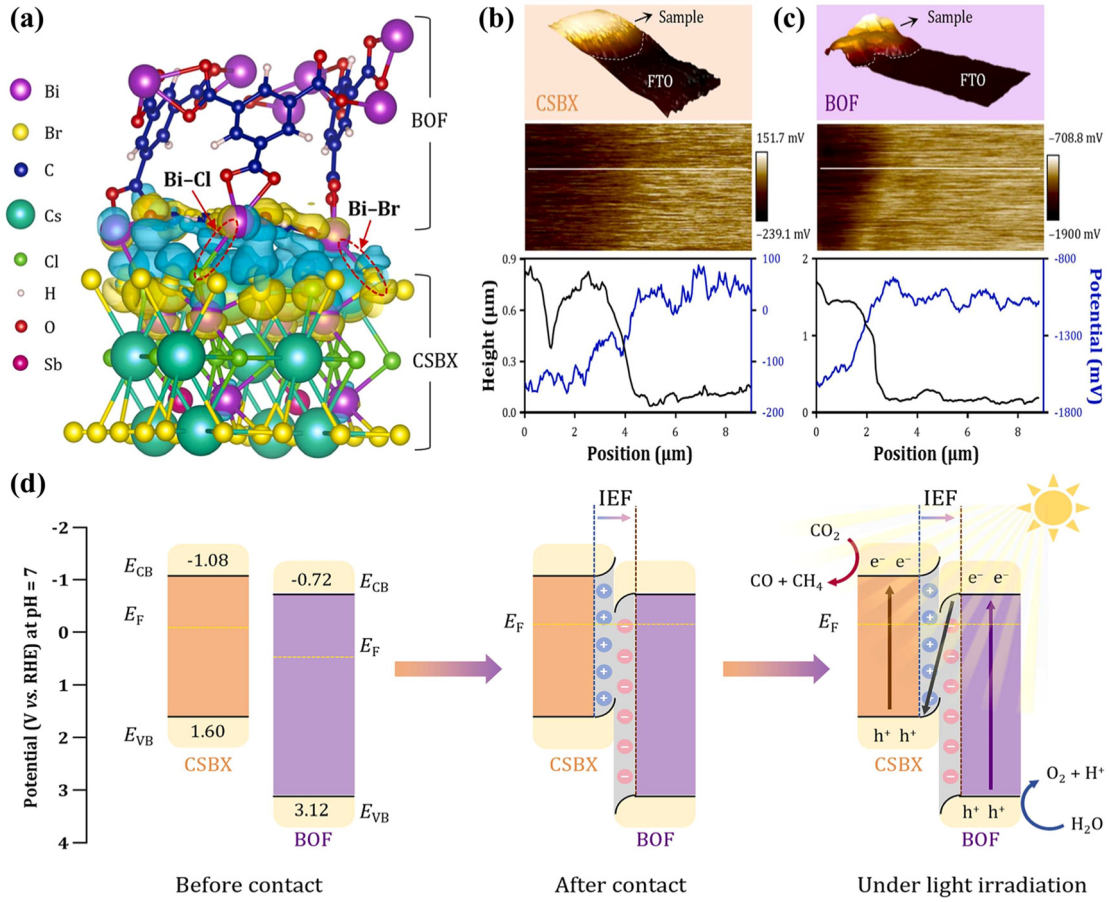


**Fig. 5** Lead-free halide-perovskite-based heterojunction: (a) charge density difference (isosurface level, 0.04 e Å$^{-3}$) over the CSBX/BOF heterojunction. The yellow and cyan regions represent the positive and negative electron density isosurfaces, respectively, KPFM surface potential images (middle), and the corresponding topography and surface potential line profiles (bottom) for (b) CSBX and (c) BOF three-dimensional topographical maps (top). (d) Schematic of the band structures of CSBX and BOF (left), interfacial charge transfer and the formation of an IEF upon hybridisation (middle), and CSBX/BOF S-scheme heterojunction under light irradiation (right). Reproduced from ref. 93, with permission of *Applied Catalysis B: Environment and Energy*, copyright 2025.

the few catalysts capable of selectively producing $C_2$ and other organic carbon products,[100] striking a balance between $^*CO$ binding and desorption, thereby enabling effective C–C coupling.

Electrocatalytic $CO_2RR$ typically occurs in an electrochemical cell, where an electrode (a metal or alloy electrode) catalyzes the reaction between $CO_2$ and $H_2$, converting them into useful chemicals. During this process, $CO_2$ is adsorbed onto the catalyst surface, where it is activated through electron transfer, generating reactive intermediates like $^*CO_2^{\bullet-}$ (a radical anion) or $^*CO_2H$ (a hydrogenated intermediate). This step requires overcoming the adsorption energy barrier between $CO_2$ and the electrode, typically occurring on metal electrodes (*e.g.*, copper, silver, gold). The reduction reaction involves the transfer of electrons and protons; electrons are delivered *via* the electrode, while protons come from the electrolyte. The electrode surface reduces $CO_2$ intermediates, generating species such as $CO_2^{\bullet-}$ or $CO_2H$.

The electrocatalytic reaction proceeds through the formation of intermediates, which are progressively reduced to final products like methanol, methane, and other hydrocarbons (Fig. 6). The overpotential, defined by the current density and voltage applied, plays a critical role in determining the product selectivity. Different electrocatalysts significantly affect the distribution of products. For instance, copper-based catalysts are often superior to others, promoting a range of carbon-containing organic products such as alkanes, alkenes, and alcohols, while silver and gold catalysts typically favor the formation of CO.

Thus, understanding and optimizing the interaction between $CO_2$ intermediates, the electronic properties of the metal catalysts, and reaction conditions are key to enhancing the efficiency and selectivity of electrocatalytic $CO_2RR$.

### 4.2 Reaction kinetics of electrocatalytic reduction

In recent years, significant progress has been made in understanding the electrocatalytic $CO_2RR$ using SACs, leading to improved catalytic performance. SACs are particularly appealing due to their high metal atom utilization, distinct electronic properties, and excellent catalytic efficiency. However, the isolated active sites in SACs can limit their effectiveness in reac-

 

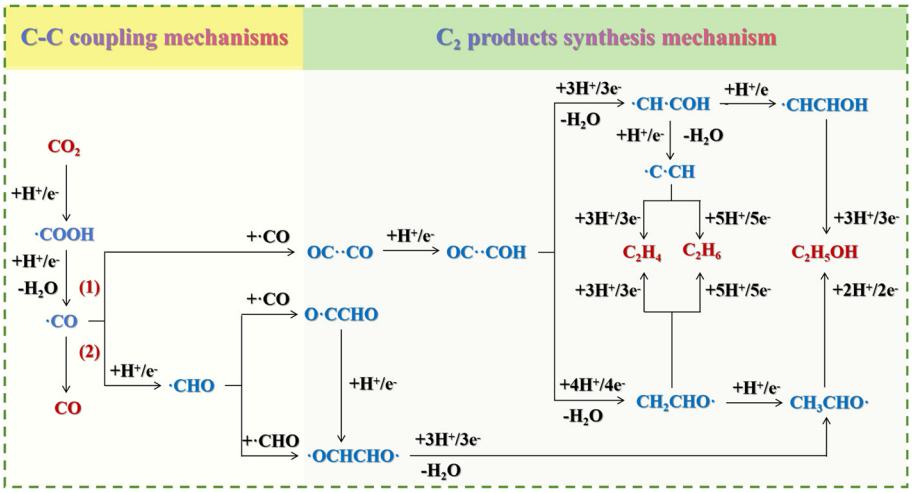


**Fig. 6** Reaction pathways of $CO_2$ reduction to produce value-added $C_2$ chemicals ($C_2H_4$, $C_2H_6$, and $C_2H_5OH$) *via* electrocatalysis by adding (1) $^*CO$ before $H^+/e^-$ and (2) $H^+/e^-$ before $^*CO$.

tions that require the simultaneous activation of multiple reactants or intermediates. To address this limitation, strategies have been developed to combine the advantages of SACs with multi-atomic sites, resulting in "fully exposed metal cluster catalysts" (FECCs).[101] These FECCs can simultaneously activate different reactants, enhancing the reaction kinetics and improving the overall electrocatalytic performance.

Recent studies[102] have demonstrated that tuning the atomic dispersion of metal species within SACs can significantly enhance the catalytic efficiency. For instance, by adjusting the pyrolysis temperature, researchers have successfully transitioned nickel (Ni) species from clusters to single-atom scales, resulting in a Ni FECC with superior $CO_2$RR performance. The optimized Ni FECC achieved a FE of up to 99% for CO production, with a CO partial current density of 347.2 mA $cm^{-2}$, and exhibited stable performance over 20 hours of electrolysis. Theoretical calculations revealed that sulfur doping plays a crucial role in regulating the charge distribution across multiple Ni sites, thus accelerating the reaction kinetics and facilitating efficient $CO_2$RR to CO.

Another study[103] focused on the development of a model Ni SAC with well-defined Ni–$N_4$ coordination on a conductive carbon support, which was used to explore the $CO_2$RR mechanism. Using advanced operando techniques, such as X-ray absorption spectroscopy, Raman spectroscopy, and near-ambient XPS, it was found that the $Ni^+$ sites in the Ni SAC were highly active for $CO_2$ activation, acting as the actual catalytic sites for the $CO_2$RR. Electrochemical kinetics studies identified the rate-determining step of the $CO_2$RR as the conversion of $^*CO_2$@ + $H^+$ → $^*COOH$, providing key insights into the mechanistic details of $CO_2$RR.

Despite the outstanding performance of SACs in $CO_2$RR, the relationship between their electronic and geometric structures and their electrocatalytic properties remains an area of ongoing investigation. Factors such as the coordination environment of metal atoms, the nature of the conductive support, and the interactions with secondary catalysts all significantly influence the efficiency and selectivity of SACs in $CO_2$RR. Understanding these structure–function correlations is critical for the rational design of SACs that exhibit high activity, selectivity, and stability.[104]

The kinetics of electrocatalytic $CO_2$RR are influenced by several key factors, including current density, applied voltage, catalyst surface properties, and the concentrations of $CO_2$ and $H_2$. Typically, the reaction rate is proportional to the current density ($j$, A $cm^{-2}$), with the reaction rate increasing as the current density increases, until a saturation point is reached. The overpotential ($\eta$) represents the difference between the required voltage for the reaction and the theoretical voltage, reflecting the activation barrier on the catalyst surface and significantly affecting the reaction rate. This relationship is often described by the Tafel equation, which characterizes the logarithmic dependence of the reaction rate on the overpotential:

$$\eta = a_{EC} + b_{EC} \cdot \log j$$

Additionally, the reaction rate ($r_{EC}$) is affected by the concentrations of $CO_2$ and $H_2$. The rate for $CO_2$RR typically follows the equation:

$$r_{EC} = k \cdot j$$

$$r_{EC} = k_{EC} \cdot (C_{CO_2})^{a_{EC}} \cdot (C_{H_2})^{b_{EC}}$$

where $C_{CO_2}$ and $C_{H_2}$ represent the concentrations of $CO_2$ and $H_2$, and $a_{EC}$ and $b_{EC}$ are the reaction orders with respect to $CO_2$ and $H_2$, and typically determined experimentally.

Overall, SACs have demonstrated remarkable potential in $CO_2$RR, with atomically dispersed active sites, tunable electronic structures, and enhanced reaction kinetics. However, challenges remain in the catalyst design, synthesis, and characterization. Future research should focus on developing novel synthetic strategies to precisely control the atomic dispersion, improving the catalyst stability under practical con-

ditions, and further elucidating the structure–activity relationships.

### 4.3 Electrocatalytic reduction of $CO_2$ using single-atom catalysts

**4.3.1 Influence of auxiliary agents on electrocatalytic performance.** SACs offer exceptional activity, selectivity, and atom efficiency, making them highly suitable for selective $CO_2$RR.[105] The performance of SACs is largely governed by the morphology and coordination environment of the metal center, typically in M–N–C structures.[106] These structures facilitate the adsorption and activation of $CO_2$, as well as the reduction process, by enabling precise control over the binding energies of key intermediates, such as $^*CO_2$, $^*COOH$, and $^*CHO$. One example is the Ni–N/NCNT catalyst developed by Kim *et al.*,[107] which achieved a FE of 96.73% for CO production in a zero-gap $CO_2$ electrolyzer with an optimized membrane electrode assembly (MEA). The asymmetrical Ni–N–C structure enhances $CO_2$ adsorption, facilitates high CO coverage, and suppresses HER, improving the $CO_2$ electroreduction activity by boosting metal utilization and $CO_2$RR efficiency.[108] In contrast, Yang *et al.*[109] demonstrated that halogen activation of metal sites can further enhance performance. Bromide, in particular, promotes the selective exposure of planar bismuth surfaces, resulting in a high current density and greater than 90% selectivity for formic acid, whereas chlorides and iodides tend to disorganize the active sites.[110]

The $CO_2$RR involves complex intermediates and competing reaction pathways, making optimization challenging. Jin *et al.*[111] addressed this by constructing atomically dispersed heterodiatomic pairs, where $^*COOH$ intermediates bridge across heteroatomic sites, lowering their formation energy. This modification enhances electron delocalization *via* Mo–Fe d–d orbital coupling, which promotes $^*CO$ desorption and improves CO selectivity. The introduction of dual- and multi-active centers has also gained attention for its ability to activate multiple reactants, improving selectivity and product diversity. For $CO_2$RR, dual-site catalysts often feature separate sites for $CO_2$ activation and subsequent hydrogenation or C–C coupling. The spatial arrangement of these sites influences the migration of intermediates, and optimizing $^*H$ coverage can help mitigate HER, improving the selectivity for $CO_2$RR over hydrogen evolution.

Single-atom alloy catalysts (SAAs) are another promising approach for $CO_2$RR to $C_{2+}$ products, although challenges remain in achieving selective C–C coupling. Cao *et al.*[112] reported on a Bi–Cu SAA catalyst that achieved 73.4% FE for $C_{2+}$ products. The interaction between Bi and Cu modulated the electronic structure of Cu, lowering the $CO_2$ adsorption and activation energy, enhancing intermediate formation, and improving the $C_{2+}$ selectivity. This study highlights the potential of SAAs in regulating active sites, and provides a new strategy for catalyst design. In a different approach, Cai *et al.*[113] used Pd atoms for $CO_2$RR to formic acid with a Pd/C–Pt/C composite electrode, demonstrating a new method for low-temperature aqueous-phase electrocatalysis. Additionally, Quan *et al.*[114] developed nitrogen-coordinated Cu SACs (Cu/NC) for $CO_2$ electrocarboxylation with styrene, achieving 92% FE and nearly 100% product selectivity for phenylsuccinic acid.

Metals such as Fe, Co, Cu, Zn, and Sn are increasingly used in $CO_2$RR due to their distinct product selectivity. Sn, In, and Pb primarily produce formic acid while effectively inhibiting HER,[115,116] whereas Zn, Au, and Ag favor CO production due to their strong interaction with the $CO^*$ intermediate, which is crucial for large-scale CO production.[117–119] However, the high cost of Au and Ag limits their practical application. Cu, as the only metal capable of producing $C_{2+}$ products, holds significant potential, as $C_2$ products (ethanol and ethylene) offer greater commercial value compared to $C_1$ products (CO and methane).[120] Despite this, the structural sensitivity of copper single atoms and their role in CC coupling remain areas of ongoing research. It has been assumed that $CO_2$RR to both CO and $C_2$ products occurs at the same Cu site, but recent studies suggest that distinct Cu sites may be involved in these steps.[121] Further mechanistic investigations are required to clarify these processes and optimize the catalyst performance. Cu-based catalysts have been extensively studied for $CO_2$RR, with various modifications improving their selectivity and efficiency. This strategy can be extended to other Lewis-acid metals to further enhance the $CO_2$RR performance. Wang *et al.*[122] developed an InBi bimetallic catalyst supported on $In_2O_3$ nanodots on $Bi_2O_2CO_3$ nanosheets, where the synergistic effect between the metals and the enhanced $CO_2$ adsorption led to 97.17% FE in an H-type electrolyzer.

Heteroatom doping, particularly with nitrogen, sulfur, or phosphorus, alters the electronic properties of the support material and enhances the SACs activity. Nitrogen-doped carbon supports improve the interaction between metal centers and $CO_2$, facilitating $CO_2$ adsorption and reduction. This doping stabilizes the metal sites and prevents agglomeration, thus improving the catalyst's stability over prolonged reactions. The coordination environment of the metal center is further optimized by the inclusion of multiple heteroatoms in the support structure. In Cu SACs, nitrogen-doped carbon support adjusts the binding strength of $^*CO$ and $^*COOH$ intermediates, enhancing $CO_2$RR to $C_2H_4$. This synergy between the metal and support is crucial for maximizing the $CO_2$RR performance. Co-catalysts, often in the form of small nanoparticles or sub-nanoclusters, have been integrated with SACs to promote cooperative catalysis. In these tandem systems, one site activates $CO_2$, while the other facilitates CO coupling, leading to higher-order products such as $C_2H_4$ and $CH_4$. Cu SACs coupled with copper nanoclusters exhibit enhanced selectivity for $C_{2+}$ products by promoting $CO_2$RR to CO, followed by coupling at the NP site.[123]

Moreover, modifying the coordination environment around the metal site further enhances the SACs performance. For instance, Cu SACs supported by $N_2$-bidentate sites in a graphdiyne structure show higher selectivity for methane production, with reduced side reactions. This design achieves a FE of 80.6% for methane and a current density of 160 mA $cm^{-2}$.[124]

 

The support curvature also affects the SACs activity. Ni SACs supported on spherical carbon materials exhibit optimized nanocurvatures, which influences the interfacial electric field, modulating intermediate adsorption during $CO_2$RR. This results in a CO partial current density of 400 mA $cm^{-2}$ at 99% FE.[125]

Cu SACs supported by nitrogen-doped carbon quantum dots (CQDs) exhibit enhanced catalytic performance, with a FE of over 80% for ethanol production and stable performance over 50 hours. This improvement stems from the atomic dispersion of Cu sites and the interaction with the nitrogen-doped support.[126]

**4.3.2 Electrocatalyst support materials.** In 2023, Cui *et al.*[127] designed an Al–Cu tandem catalyst supported on carbon nanotubes (CNTs) to improve $CH_4$ production *via* efficient $CO_2$RR and enhanced electron transfer, significantly boosting the $CH_4$ selectivity. This catalyst system uses the complementary properties of Al and Cu, facilitating the conversion of $CO_2$ and increasing the overall efficiency of methane production. Similarly, Ding *et al.*[128] developed a cascade catalyst combining $SnS_2$ nanosheets with single-atom Sn, achieving 82.5% ethanol selectivity. In this system, $CO_2$ is first reduced to formic acid on $SnS_2$, followed by bicarbonate formation at the single-atom Sn sites, where C–C coupling occurs *in situ* to yield ethanol. This mechanism exemplifies the synergy between different catalytic sites and materials, promoting high selectivity for desired products.

While precious metals such as Ru, Pd, and Pt have demonstrated high efficiency in $CO_2$RR, their high cost and limited scalability prompt the exploration of more affordable and scalable SACs.[129–131] Liu *et al.*[132] developed a Sn–Cu diatomic catalyst by introducing Sn into isolated Cu sites, which achieved a FE of 99.1% for CO production.[133] The high efficiency of this catalyst is attributed to its efficient atom utilization, SMSI, and the high unsaturation of the coordination environment around the metal atoms. Additionally, the nitrogen-doped porous carbon support improves mass transfer, ensuring that the catalyst can maintain high performance over extended periods.

Su *et al.*[134] reported a Cu/Zn hierarchical porous catalyst that inhibits HER, while favoring alcohol formation. This catalyst enhances intermediate interactions with the surface. Furthermore, it features a porous structure that increases the density of surface active sites and improves the surface-to-volume ratio, promoting the formation of $C_2$ products. In another study, Chen *et al.*[135] employed a $Cu^{2+}$ electrolyte to balance Cu ion dissolution and deposition, achieving 83.3% ethylene selectivity after 4 hours of electrolysis.[136] The periodic removal of accumulated bicarbonate during the reaction further stabilized the catalyst, maintaining high performance and selectivity. The combination of ultrafast thermal shock synthesis and pore engineering enhanced the electrode's reactive surface area, facilitated charge transfer, and improved selectivity, ultimately boosting the catalyst's overall efficiency. Fan *et al.*[137] addressed stability concerns in acidic systems by modifying the electrode surface with benzimidazole-functionalized ionomer groups. This modification activated $CO_2$ and enhanced C–C coupling, achieving over 80% multi-carbon selectivity. The control of the microscopic water environment and the improvement of the catalyst stability under acidic conditions further contributed to the high performance.

Oxygen or nitrogen vacancies in the support material can improve metal–support interactions and increase the number of available active sites. Supports like $TiO_2$ or carbon materials with oxygen vacancies can stabilize metal sites and facilitate electron transfer, lowering the activation energy for $CO_2$RR. This enhances the reaction rates and improves selectivity for valuable products such as $C_{2+}$ compounds. Using $Ti_3C_2O_2$-based MXene supports showed that the asymmetric coordination of the metal center improved $CO_2$RR and product selectivity. The support's ability to modulate the metal's electronic properties and interaction with intermediates contributed to enhanced catalytic activity, such as improved formic acid production.[138]

The chemical composition of the carrier is also important. Nitrogen-doped carbon supports, for instance, can enhance the electronic environment of SACs, improving $CO_2$ adsorption and the formation of $C_{2+}$ products. Supports with high surface area and tunable porosity, such as MOFs, are ideal for dispersing metal atoms uniformly, improving accessibility to reactants and boosting the catalyst efficiency.[139]

Tandem catalysis, where SACs are combined with nanoclusters or sub-nanometric catalysts, can further enhance performance. These hybrid systems allow for cooperative interactions, where one component activates $CO_2$ and the other facilitates CO coupling to form higher-order products. Cu-based SACs combined with copper nanoclusters show improved selectivity for $C_{2+}$ products due to this synergy.[123] The stability of SACs is also influenced by the support. Conductive and stable supports, like graphene or carbon nanotubes, help maintain the high dispersion of metal atoms and ensure efficient electron transfer, preventing aggregation and preserving catalytic activity. A study of CuFONC, a carbon composite with Cu single atoms supported by F, O, and N-doped motifs, found that the carrier stabilized the Cu sites, enhancing CO–C coupling and selectivity for $C_2$ products. The carrier's chemical environment strengthened the interaction between Cu and CO intermediates, leading to an FE of 80.5%.[140] The curvature of the carrier also plays a role. Ni SACs on spherical carbon exhibited superior $CO_2$ reduction performance due to the stronger electric fields generated by the nanocurvature. These fields help optimize the adsorption of intermediates, enhancing the SACs activity.[125]

Overall, these studies demonstrate the effectiveness of SACs in $CO_2$RR, highlighting various strategies for improving the efficiency, selectivity, and stability. The use of different metal combinations, such as Cu–Sn, Cu–Bi, and Cu–Zn, as well as modifications to support structures and electrolyte conditions, plays a critical role in tailoring the catalytic properties and enhancing the overall $CO_2$RR. The transition to more affordable, scalable SACs is essential for advancing $CO_2$RR technologies, with significant potential for commercial applications in producing valuable carbon-based products.[141]

**4.3.3 Graphene-structured electrocatalysts.** Graphene-based SACs offer significant advantages for $CO_2$RR due to their excellent electronic conductivity, high surface area, and the ability to fine-tune the local electronic environment of active sites. The key to enhancing the catalytic activity of graphene-based SACs lies in the design of graphene's structure, particularly through defect engineering, heteroatom doping, and the creation of 3D graphene (3DGr) architectures. The 3D structure of graphene not only prevents issues such as re-stacking observed in 2D graphene, but also improves mass and electron transport, essential for efficient $CO_2$RR. The introduction of defects and heteroatoms (*e.g.*, nitrogen, sulfur) in the graphene matrix further modifies the electronic properties of the catalyst, enabling better activation of $CO_2$ and stabilization of the reaction intermediates.

The modification of the graphene matrix plays a critical role in improving the selectivity and efficiency of $CO_2$RR. For example, nitrogen doping and the introduction of vacancy defects have been shown to modulate the electronic environment, optimizing the charge distribution at the active sites. In iron-based SACs supported on nitrogen-doped graphene (Fe–N–C), nitrogen plays a key role in lowering the $CO_2$RR onset potential and widening the potential range for achieving high CO FE. This is due to the enhanced charge capacity of the $^*$COOH intermediate, which facilitates selective $CO_2$RR over competing reactions like hydrogen evolution. Additionally, the introduction of defects provides additional catalytic sites, improving reactivity while maintaining the material's structural integrity (Fig. 7).[142,143]

Another significant aspect of graphene-based SACs is the tailored design of the interfacial microenvironment (Fig. 7). For instance, in CoPc catalysts supported on a graphitic carbon nitride/graphene ($C_3N_4$/G) matrix, the graphene matrix enriches $CO_2$ and dissociates $H_2O$ to produce active hydrogen species, further enhancing the catalytic performance. The interaction between $C_3N_4$ and graphene also optimizes the electronic properties of the active sites, leading to a higher turnover frequency (TOF) and exceptional CO selectivity, with a FE consistently above 98%.[144] These findings highlight the importance of both structural and compositional engineering in graphene-based SACs, demonstrating that the manipulation of defects, doping, and microenvironment tuning are essential for improving the $CO_2$RR performance.

Thus, the combination of hierarchical graphene structures, defects, heteroatom doping, and interfacial microenvironment design results in SACs with enhanced catalytic stability, product selectivity, and $CO_2$RR efficiency. These strategies are crucial for advancing the development of efficient and high-performance catalysts for $CO_2$ conversion.

# 5 Thermocatalytic $CO_2$ reduction based on Fischer–Tropsch synthesis

## 5.1 Reaction kinetics and mechanism of Fischer–Tropsch synthesis

The FTS mechanism for $CO_2$ hydrogenation on SACs involves several key stages: adsorption of $CO_2$, activation *via* hydrogenation, and product formation through well-defined pathways. The reaction starts with the adsorption of $CO_2$, which is then hydrogenated to form active intermediates such as $^*$CO, methanol, or methane. This process typically follows a surface adsorption–reaction–desorption cycle. Temperature plays a crucial role in these reactions; FTS generally occurs at elevated temperatures (300–500 °C), where the reaction heavily relies on thermal energy to overcome activation barriers. $CO_2$ hydrogenation to olefins and other FTS products is an exothermic reaction, with low temperatures favoring product formation, while higher temperatures enhance the reaction kinetics. In practice, unreacted syngas is often recycled to optimize conversion. High pressure conditions also favor olefin formation. The reaction equations of $CO_2$ hydrogenation to alkane, olefin and alcohol are shown in the following formulas:

$$CO_2 + H_2 \leftrightarrow CO + H_2O$$

$$CO + 2H_2 \rightarrow \frac{1}{n}C_nH_{2n} + H_2O$$

$$CO + \frac{2n+1}{n}H_2 \rightarrow \frac{1}{n}C_nH_{2n+2} + H_2O$$

$$CO + 2H_2 \rightarrow \frac{1}{n}C_nH_{(2n+1)}OH + \frac{n-1}{n}H_2O$$

The reaction rates in FTS follow the Arrhenius equation, where the rate is exponentially dependent on temperature:

$$r_{FTS} = A \cdot e^{-\frac{E_a}{RT}}$$

Here, $r_{FTS}$ is the reaction rate, $A$ is the pre-exponential factor, $E_a$ is the activation energy, $R$ is the gas constant, and $T$ is the absolute temperature. The reaction rate also depends on the concentrations of $CO_2$ and $H_2$, with the dependence often described by a power-law expression:

$$r_{FTS} = k_{FTS} \cdot (C_{CO_2})^{a_{FTS}} \cdot (C_{H_2})^{b_{FTS}}$$

$$r_{FTS} = k_{FTS} \cdot (C_{CO_2})^{a_{FTS}} \cdot (C_{H_2})^{b_{FTS}} \cdot e^{-\frac{E_a}{RT}}$$

where $k_{FTS}$ is the rate constant, and $a_{FTS}$ and $b_{FTS}$ are the reaction orders with respect to $CO_2$ and $H_2$, respectively. Higher reactant concentrations typically increase the reaction rate, particularly at elevated temperatures.

At lower temperatures, the reaction is often limited by electron transfer and hydrogenation steps. At higher temperatures, the rate is more influenced by the activation energy. Temperature adjustments allow for selective production of the desired products: lower temperatures favor methane, while higher temperatures promote olefin and alcohol formation.

The reaction mechanism varies depending on the catalyst and temperature. For Fe-based catalysts, the active phase has shifted from metallic iron to the $FeC_x$ phase in recent studies,[145] following the Mars-van Krevelen (MvK) mechanism. This mechanism divides the reaction into the surface and outer layers of the catalyst, with fast reactions following the Langmuir–Hinshelwood (L–H) pathway, where most of the FTS activity occurs at a small fraction of active sites. The slow

 

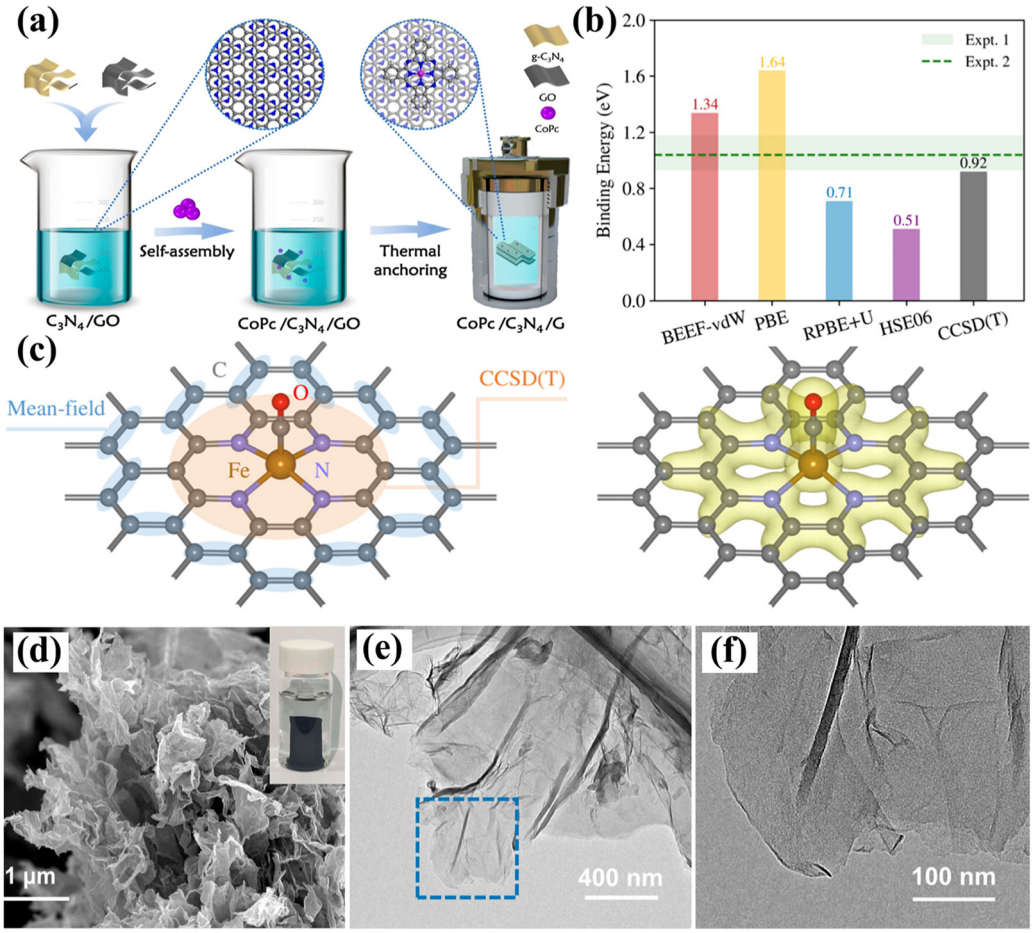


**Fig. 7** Illustration and benchmark of the local embedding for modeling single-atom catalysts, along with the synthesis procedure and morphology characterization: (a) schematic of the synthesis process of $CoPc/C_3N_4/G$,[142] (b) binding energies of CO on $FeN_4$ predicted using DFT with four functionals (BEEF-vdW, PBE, RPBE+U, and HSE06) and CCSD (T) local embedding. Experimental TPD measurements of the CO binding energy are 0.93–1.18 eV and 1.04 eV,[143] (c) schematic showing fragment selection in local embedding calculations (left) and electron density of the $FeN_4C_{10}$-embedded fragment (right), (d–f) SEM, TEM, and HR-TEM images of $CoPc/C_3N_4/G$.[143] Reproduced from ref. 142 and 143, with permission of ACS Catalysis, copyright 2024.

pathway, governed by the MvK mechanism, occurs predominantly at the majority of active sites.[146]

Brübach *et al.*[147] explored the kinetics of $CO_2$ hydrogenation over Fe-based catalysts, identifying key inhibitory factors such as the strong adsorption of oxygen-containing species and the effects of shifting the equilibrium to lower CO partial pressures. They proposed new kinetic expressions based on the L–H model, which incorporate these dynamics.

$$r_{\mathrm{RWGS}} \approx \frac{k_{\mathrm{RWGS}}\left(p_{\mathrm{H_2}}^{0.5}p_{\mathrm{CO_2}} - \dfrac{p_{\mathrm{CO}}p_{\mathrm{H_2O}}}{K_{\mathrm{eq}}p_{\mathrm{H_2}}^{0.5}}\right)}{\left(1 + a_{\mathrm{RWGS}}\dfrac{p_{\mathrm{H_2O}}}{p_{\mathrm{H_2}}}\right)^2}$$

$$r_{\mathrm{FT}} \approx \frac{k_{\mathrm{FT}}p_{\mathrm{CO}}p_{\mathrm{H_2}}}{\left(1 + a_{\mathrm{FT}}\dfrac{p_{\mathrm{H_2O}}}{p_{\mathrm{H_2}}} + p_{\mathrm{CO}}b_{\mathrm{FT}}\right)^2}$$

Product distribution in $CO_2$ hydrogenation typically follows the Anderson–Schulz–Flory (ASF) model:

$$W_n = n(1+\alpha)^2\alpha^{n-1}$$

where $n$ is the carbon number, $W_n$ is the mass fraction of hydrocarbons with $n$ carbon atoms, and $\alpha$ is the chain growth probability.

The integration of reaction kinetics models with ML and DL is an emerging direction for uncovering unknown mechanisms. Sun *et al.*[148] employed a combined approach of artificial neural networks (ANN) and response surface methodology (RSM) to simulate the product distribution of FTS in a microchannel reactor. The model demonstrated the ability to predict the formation rates of hydrocarbon products in the $C_2$–$C_{15}$ range, as well as the olefin-to-paraffin ratio (OPR), showing advantages in rapid convergence and high predictive accuracy. This approach offers a novel perspective for studying the kinetics of complex catalytic processes. Wang *et al.*[149] developed a radial basis function neural network (RBFNN), which offers fast convergence and reduced computation time, to generate

data matrices with a limited set of experimental data. A comprehensive kinetic model, coupled with a genetic algorithm (CKGA), was used to select mechanisms and infer potential reaction pathways. The RSM-based RBFNN, constructed *via* central composite design, processed responses and subsequent singular/multiple optimizations to produce the data matrix. This approach provides a highly practical and valuable tool for process engineering design and practice, especially for understanding product distribution during FTS (Fig. 8).

### 5.2 Single-atom catalysts in $CO_2$ conversion *via* Fischer–Tropsch synthesis

The synthesis of SACs for $CO_2$ hydrogenation typically involves the reduction of metal precursors to isolated metal atoms, which are subsequently dispersed onto supports through thermal or chemical reduction. The catalytic performance of SACs is strongly influenced by strong metal–support interactions (SMSI), which stabilize metal atoms and facilitate the activation of $CO_2$ and $H_2$. These interactions play a crucial role in determining the reaction pathway and product selectivity. Notably, the metal's d-band structure modulates the adsorption and activation of CO, ultimately affecting the product distribution. For instance, $Co_1/W_6S_8$ favors the formation of $C_{2+}$ hydrocarbons,[150] whereas $Ni_1/W_6S_8$ exhibits higher selectivity toward methanol, highlighting the critical role of metal–support interactions in controlling the reactivity and selectivity.

Iron-based SACs, particularly those supported on $CeO_2$, further exemplify the influence of support interactions and preparation conditions on catalytic performance. Wang *et al.*[151] demonstrated that iron species can be effectively dispersed on $CeO_2$ *via* the deposition–precipitation method, forming $Fe^{\delta+}$ single atoms under $CO_2$ hydrogenation conditions (300 °C, 2 MPa). These single atoms are stabilized through Fe–O–Ce bonds, which play a key role in $CO_2$ activation. Additionally, co-doping with Ru enhances the iron dispersion and prevents metal aggregation under reaction conditions, thereby stabilizing the catalyst and modulating the electronic environment of the active sites.

The $CO_2$ hydrogenation reaction on SACs proceeds through the adsorption of $CO_2$ and $H_2$ onto metal atoms, leading to protonation and electron transfer, forming intermediates such as $^*CO$ and $^*HCOOH$. The binding strength of $CO_2$ and its intermediates is a critical factor in determining the reaction mechanism and product distribution. Metal–support interactions, particularly those involving reducible oxides such as $CeO_2$, facilitate electron transfer and optimize the binding energies of the reaction intermediates, thereby influencing the catalytic selectivity.

In conclusion, the rational design of SACs for $CO_2$ hydrogenation necessitates precise control over metal dispersion,

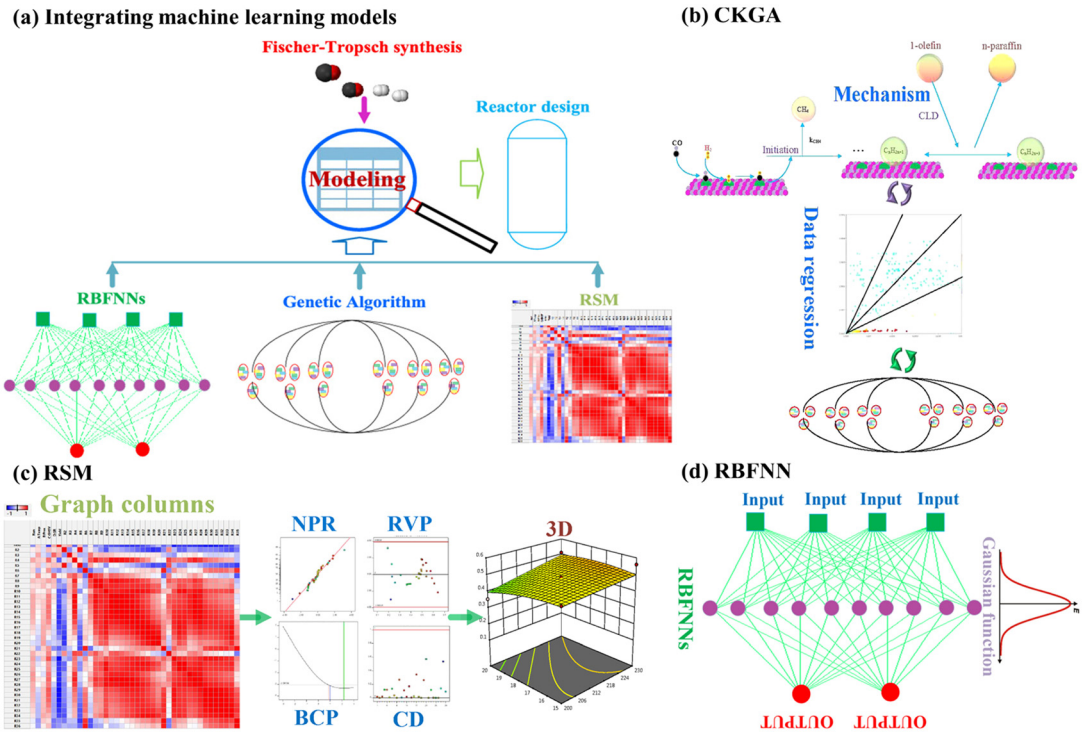


**Fig. 8** Machine learning assists in unveiling the reaction kinetics process: (a) integrating machine learning models, (b) schematic of the genetic algorithm (GA) for mechanism discrimination and data regression (CLD refers to chain-length dependent), (c) schematic of RSM for significance analysis (NPR refers to a normal plot of residues, RVP refers to residues *versus* predictions, BCP refers to the Box-Cox plot for power transform, and CD refers to Cook's distance), (d) schematic of RBFNN formulated from the Gaussian function. Reproduced from ref. 149, with permission of ACS OMEGA, copyright 2021.

 

oxidation state, and metal–support interactions. Co-doping strategies, such as incorporating Ru, improve metal dispersion and enhance the stability of active sites under reaction conditions. The optimization of metal–support interactions, particularly by tuning the metal's d-band structure, is essential for achieving superior catalytic activity and selectivity.

## 6 Advanced strategies for single-atom catalysts innovation in $CO_2$ reduction

Recent advancements in SACs have demonstrated their significant potential in enhancing $CO_2$RR, offering exceptional atomic efficiency and tunable catalytic sites. By maximizing atomic utilization, SACs ensure that each active site corresponds to a single metal atom, thereby substantially enhancing catalytic efficiency compared to conventional nanoparticle-based catalysts. This atomic-level precision, combined with the ability to finely tune the electronic structure and coordination environment of active sites, facilitates efficient $CO_2$ activation and reduction. SACs have been shown to catalyze the formation of key small organic molecules, such as formate, carbon monoxide, and methane, through mechanisms involving $CO_2$ adsorption, electron transfer, and bond cleavage.

Despite these promising advancements, a comprehensive mechanistic understanding of SAC-mediated $CO_2$RR remains incomplete. Current knowledge of precise reaction pathways, the identification of key intermediates, and the role of atomic coordination in determining catalytic activity remains limited. Gaining deeper insights into these mechanistic aspects is crucial for optimizing SACs for large-scale applications. A fundamental understanding of the reaction mechanisms will enable the rational design of SACs with enhanced stability, selectivity, and efficiency-critical attributes for achieving sustainable $CO_2$RR and contributing to global carbon neutrality objectives.

Furthermore, SACs represent a paradigm shift from conventional catalysts, which typically consist of supported metal or metal oxide nanoparticles. The unique atomic-scale structure of SACs facilitates novel reaction pathways that differ significantly from those of traditional catalysts. These distinct reaction dynamics are crucial for advancing $CO_2$RR, enabling more efficient conversion and improved product selectivity.

This integrated framework, as shown in Fig. 9, enables the precise design and optimization of SACs, paving the way for scalable and efficient $CO_2$ conversion.

The performance of SACs is fundamentally governed by their structural design, which directly impacts the catalytic activity and selectivity. This review introduces an innovative approach for $CO_2$RR, where experimental data guide the selec-

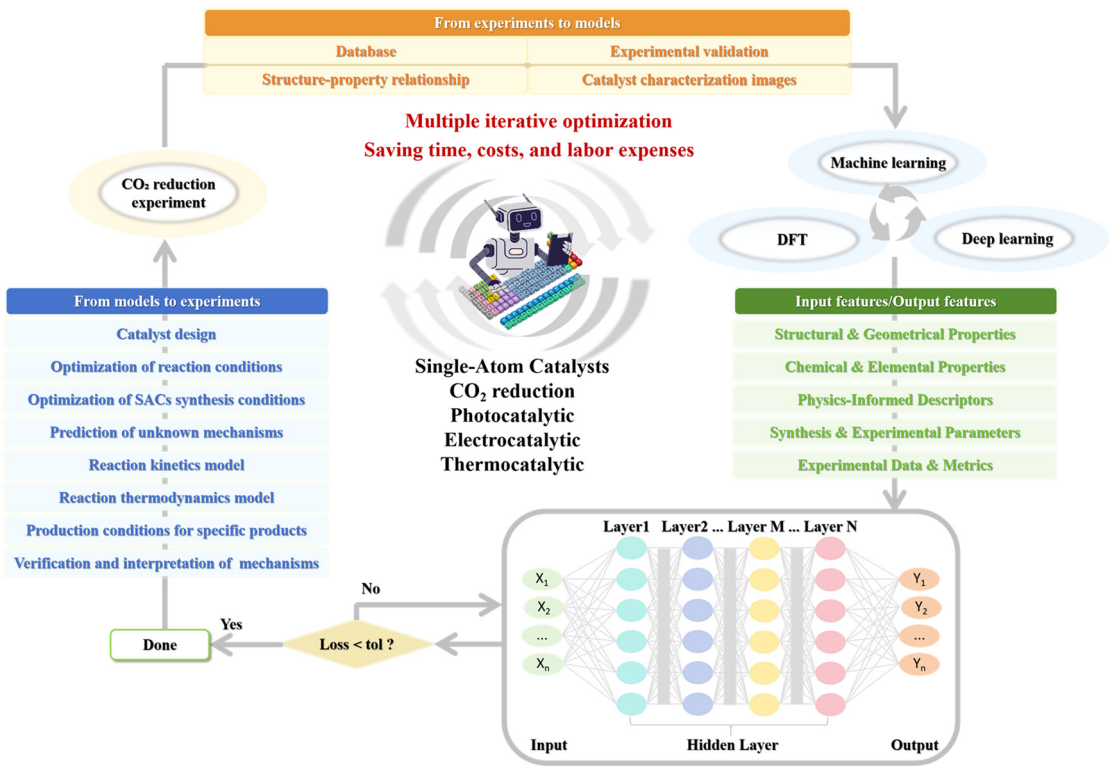


**Fig. 9** Holistic iterative optimization framework for $CO_2$ reduction using single-atom catalysts: integrating advanced machine learning, deep learning, DFT, reaction kinetics and thermodynamic models, high-throughput experimental feedback, and Bayesian optimization for the rational design and enhancement of catalytic performance and mechanistic insights.

tion of reaction conditions, preparation methods of SACs, and key microstructural features. These factors serve as critical parameters in ML models and DFT calculations. By developing mechanistic models based on reaction kinetics and thermodynamics, we aim to iteratively refine active learning models, self-supervised learning frameworks, and large-scale predictive models. In combination with multimodal models, high-throughput experimental data and material characterization results are used to uncover the relationship between the catalyst structure, catalytic properties, reaction pathways, and intermediate selectivity. These efforts reveal previously unexplored $CO_2$RR mechanisms, providing valuable insights into the rational design of SACs for the highly selective production of target chemicals. Furthermore, by applying Bayesian optimization principles, we propose a strategy to enhance the experimental outcomes, enabling continuous iteration between model predictions and experimental validation.

### 6.1 Optimization of catalyst synthesis in structure and conditions

The catalytic hydrogenation of $CO_2$ encompasses multiple pathways, including thermocatalytic, electrocatalytic, photocatalytic, and photo-electrocatalytic reduction. Among these, thermocatalysis has reached a relatively advanced stage of industrial application, while electrocatalytic and photocatalytic systems remain largely confined to laboratory research.

Photocatalysis, inspired by natural photosynthesis, provides an alternative approach for $CO_2$RR, offering advantages such as low energy consumption and high flexibility. However, photocatalytic systems currently face limitations, including low conversion efficiency and high costs associated with photovoltaic systems. Challenges such as poor interfaces, crystal lattice mismatches, and dangling bonds still limit the performance of photocatalytic and electrocatalytic materials.

Electrocatalysis presents several advantages, including the ability to operate under mild reaction conditions (ambient temperature and pressure) and the flexibility to modulate intermediate species. These features make electrocatalysis a promising option for scalable $CO_2$RR. However, high costs associated with electrocatalytic systems, particularly expensive materials used in catalysts and electrodes, pose significant barriers to commercialization.

Future research should focus on developing advanced materials to address the fundamental limitations of these systems. For example, low-dimensional semiconducting materials are promising for constructing high-quality interfaces with well-aligned band gaps, facilitating efficient light absorption and charge transfer. The integration of van der Waals heterostructures into photoelectrodes can enhance exciton dissociation, enabling more efficient electron and hole transfer to the catalyst's active sites, thereby improving the overall catalytic performance. Optimizing reaction conditions —such as the temperature, pressure, and $CO/H_2$ ratio—will be crucial for enhancing the catalytic efficiency of SACs. Particular attention should be paid to the design of new support materials, such as perovskite-based structures, to regulate metal–support interactions. These innovations will enable better control over the electronic properties and coordination environments of SACs, improving the selectivity and efficiency of $CO_2$ reduction.

Overall, while SACs have shown significant promise in $CO_2$ hydrogenation and other critical reactions, addressing the remaining challenges related to the cost, reaction conditions, and mechanistic understanding is essential for large-scale implementation of SACs in sustainable $CO_2$ reduction. Continued improvement in both the fundamental understanding of SACs and the development of new materials will help achieve more efficient, cost-effective, and scalable solutions for $CO_2$ utilization, advancing scientific innovation and global sustainability goals.

### 6.2 Machine learning-driven design and pathways of single-atom catalysts for $CO_2$ reduction

The use of SACs for $CO_2$ reduction into valuable chemicals has attracted significant attention due to their potential to reduce carbon emissions and store renewable energy. Achieving high selectivity and efficiency in $CO_2$RR necessitates a comprehensive understanding of the reaction mechanisms, active sites, and intermediate species involved. By integrating ML with DFT calculations, this approach has emerged as a powerful tool for elucidating the reaction mechanisms, optimizing the catalyst design, and predicting reaction pathways.

ML techniques, including DL, active learning, and self-supervised learning, facilitate the prediction of key catalytic properties, such as intermediate adsorption energies, binding affinities, and the electronic structures of SACs. Analyzing large datasets enables ML models to uncover correlations between the catalyst composition, support materials, and catalytic performance, offering valuable insights into designing highly selective SACs for specific high-value $CO_2$RR products. Notably, ML can guide the design of SACs with tailored properties, such as optimized metal–support interactions and atomic arrangements, thereby improving the reaction pathways and catalytic efficiency.

Integrating ML models with multi-modal data, such as structural and operational information derived from techniques like electron microscopy, further advances the comprehension of catalytic systems. This integration aids in designing SACs with specific properties that optimize the reaction mechanisms and enhance the catalytic performance. For instance, in Cu-based SACs, ML models have been employed to control the morphology of metal nanoparticles, which, in turn, influences the reaction mechanism and product distribution, thereby improving the $CO_2$RR performance.

Despite the promise of ML in catalyst design, several challenges remain. A major hurdle is the lack of high-quality, annotated datasets for effective ML model training. Data scarcity and experimental noise often lead to inaccurate predictions, hindering the development of optimal catalysts. Furthermore, ML models struggle to capture the full complexity of catalytic systems, especially non-equilibrium effects that influence the SACs stability and reactivity. To overcome these

 

challenges, future research should focus on expanding and refining datasets through high-throughput experimental techniques and advanced simulations. Hybrid approaches combining data-driven ML methods with first-principles calculations, such as ML-DFT, could further enhance the prediction accuracy and reliability. Another limitation of the current ML models is their limited interpretability. While ML can accurately predict the catalytic properties, understanding the underlying physical mechanisms remains a significant challenge. Enhancing the transparency of ML models through explainable AI techniques is crucial for gaining deeper insights into the catalytic processes and guiding the rational design of SACs with improved performance.

Coupling ML with *operando* techniques, such as X-ray spectroscopy and electron microscopy, facilitates the real-time monitoring of active sites and structural dynamics during reactions. This real-time analysis provides valuable insights into the formation of reaction intermediates and the evolution of active sites throughout the $CO_2$RR process, offering a deeper understanding of the catalytic behavior of SACs.

While ML models hold great promise for advancing the design and optimization of SACs for $CO_2$RR, addressing challenges related to the data quality, model interpretability, and system complexity is essential for realizing their full potential. Integrating ML with high-throughput experimentation, advanced simulations, and operando techniques will pave the way for the development of more efficient and selective SACs, ultimately advancing $CO_2$RR technologies and contributing to global sustainability goals.

### 6.3 Synergistic optimization of catalysts *via* machine learning and experimental validation

Developing SACs for $CO_2$RR requires integrating advanced ML, DFT, and experimental validation to enhance the catalyst performance and optimize the reaction pathways. The synergy between predictive models and experimental data provides deeper mechanistic insights, guiding the rational design of SACs with high selectivity and efficiency.

To elucidate the reaction mechanisms of SACs and identify the active phases in $CO_2$RR, both computational and experimental approaches must be integrated. Computational techniques such as DFT predict the electronic structure of active sites, adsorption energies, and reaction intermediates. By incorporating ML models (*e.g.*, RF, DL, and transformer models), these predictions enable the accurate identification of key catalytic properties and reaction pathways. Optimization of SACs can be achieved by selecting the appropriate descriptors for catalysts, auxiliary agents, and support materials, with a focus on tailoring the spatial structure to enhance the catalytic performance.

Bayesian theory provides a robust framework for constructing thermodynamic and kinetic models based on experimental data, facilitating the prediction of highly selective, efficient, and stable SACs. Integrating these predictions with experimental validation enables iterative model refinement. Incorporating new experimental data enhances the predictive accuracy, facilitating the development of more precise models. This continuous feedback loop between the computational predictions and experimental testing is crucial for uncovering previously unknown reaction pathways and optimizing SACs for $CO_2$RR. Furthermore, by continuously updating models with new data and refining reaction mechanisms, optimal reaction conditions for specific products can be predicted. The iterative optimization process enables tailored SACs design, adjusting the catalyst structures and reaction environments based on the desired product distribution.

The dynamic interplay between the ML predictions, DFT simulations, and experimental validation accelerates SACs development, ensuring more efficient and selective $CO_2$RR. The continuous refinement of computational models and experimental methodologies deepens mechanistic understanding, facilitates the design of highly selective SACs, and optimizes reaction conditions, ultimately advancing scalable catalytic applications.

## 7 Conclusion

SACs have shown great potential in $CO_2$RR due to atomically dispersed active sites, which allow for tunable catalytic properties. However, further development is necessary to fully understand the reaction mechanisms, optimize conditions, and scale up the catalysts. The integration of DFT, ML, and experimental validation holds immense promise for designing next-generation SACs with improved efficiency, selectivity, and stability.

1. The synergy between DFT and ML has greatly advanced the SACs design for $CO_2$RR. DFT provides insights into the electronic structure and reaction intermediates, while ML optimizes the catalyst properties, predicts the reaction pathways, and tailors the SACs functionalities to enhance both efficiency and selectivity.

2. Iterative ML refinement through continuous experimental validation creates a dynamic feedback loop, progressively improving SACs. Integrating experimental data enhances the prediction accuracy, enabling the design of SACs with superior stability and selectivity for specific products.

3. Achieving deeper mechanistic understanding requires precise identification of active sites. Combining ML, DFT, and experimental techniques helps elucidate complex reaction pathways, optimizing the SACs coordination environments and improving selectivity.

4. The SACs design must account for the different reaction conditions, such as temperature, pressure, and $CO/H_2$ ratios. Fine-tuning these parameters alongside well-designed SACs enhances the catalytic performance and stability under practical conditions.

5. Multimodal modeling, combining DFT structural descriptors with experimental data, allows for precise control over the SACs active sites and configurations, facilitating the development of highly active and scalable catalysts for industrial $CO_2$RR applications.

These advancements are crucial for realizing practical $CO_2$RR technologies and achieving global sustainability goals.

## Data availability

No primary research results, software or code have been included, and no new data were generated or analysed as part of this review.

## Conflicts of interest

There are no conflicts to declare.

## Acknowledgements

We ackowledge the financial support from China NSFC No.22276026 received by Prof. Lifen Liu.

## References

1 T. J. Wang, W. S. Fang, Y. M. Liu, F. M. Li, P. Chen and Y. Chen, Heterostructured Pd/PdO nanowires for selective and efficient $CO_2$ electroreduction to CO, *Energy Chem.*, 2022, **70**, 407–413.
2 W. Wang, Z. Ma, X. Fei, X. Wang, Z. Yang, Y. Wang, J. Q. Zhang, H. Ning, N. Tsubaki and M. B. Wu, Joint tuning the morphology and oxygen vacancy of $Cu_2O$ by ionic liquid enables high-efficient $CO_2$ reduction to $C_2$ products, *Chem. Eng. J.*, 2022, **436**, 135029.
3 W. Wang, X. Wang, Z. Ma, Y. Wang, Z. Yang, J. Zhu, L. Lv, H. Ning, N. Tsubaki and M. Wu, Carburized $In_2O_3$ Nanorods Endow $CO_2$ Electroreduction to Formate at 1 A $cm^{-2}$, *ACS Catal.*, 2022, **13**, 796–802.
4 Y. Yang, S. Louisia, S. Yu, J. Jin, I. Roh, C. Chen, M. V. Fonseca Guzman, J. Feijóo, *et al.*, Operando studies reveal active Cu nanograins for $CO_2$ electroreduction, *Nature*, 2023, **614**, 262–269.
5 Z. Feng, X. Zhu, J. Yang, K. Zhong, Z. Jiang, Q. Yu, Y. Song, Y. Hua, H. Li and H. Xu, Inherent Facet-Dominant effect for cobalt oxide nanosheets to enhance photocatalytic $CO_2$ reduction, *Appl. Surf. Sci.*, 2022, **578**, 151848.
6 R. Murakami, K. Shiota, A. Uchida and F. Inagaki, Light-swing $CO_2$ capture: photoirradiation-based chemical $CO_2$ release based on photoisomerization of azobenzene-amine/guanidine derivatives, *Green Chem.*, 2024, **26**, 7406.
7 S. S. Satter, J. S. Lopez, M. L. Hubbard, Y. Jiang, R. A. Dagle and J. Kothandaraman, Reactive direct air capture of $CO_2$ to C-C coupled products using multifunctional materials, *Green Chem.*, 2024, **26**, 8242–8255.
8 J. X. Gu, X. Zhao, Y. Sun, J. Zhou, C. Y. Sun, X. L. Wang, Z. H. Kang and Z. M. Su, A photo-activated process cascaded electrocatalysis for the highly efficient $CO_2$ reduction over a core–shell ZIF-8@Co/C, *J. Mater. Chem. A*, 2020, **8**, 16616–16623.
9 L. Ye, Y. Ying, D. Sun, Z. Zhang, L. Fei, Z. Wen, J. Qiao and H. Huang, Highly Efficient Porous Carbon Electrocatalyst with Controllable N–Species Content for Selective $CO_2$ Reduction, *Angew. Chem., Int. Ed.*, 2020, **59**, 3244–3251.
10 C. X. Zhao, J. N. Liu, B. Q. Li, D. Ren, X. Chen, J. Yu and Q. Zhang, Multiscale Construction of Bifunctional Electrocatalysts for Long-Lifespan Rechargeable Zinc-Air Batteries, *Adv. Funct. Mater.*, 2020, **36**, 2003619.
11 Y. Zhou, Z. Wang, L. Huang, S. Zaman, K. Lei, T. Yue, Z. Li, B. You and B. Y. Xia, Engineering 2D Photocatalysts toward Carbon Dioxide Reduction, *Adv. Energy Mater.*, 2021, **11**, 2003159.
12 O. S. Bushuyev, P. D. Luna, C. T. Dinh, J. Lagemaat, S. O. Kelley and E. H. Sargent, What Should We Make with $CO_2$ and How Can We Make It?, *Joule*, 2018, **2**, 825–832.
13 J. M. Spurgeon and B. A. Kumar, comparative technoeconomic analysis of pathways for commercial electrochemical $CO_2$ reduction to liquid products, *Energy Environ. Sci.*, 2018, **11**, 1536–1551.
14 Y. Y. Birdja, E. Pérez-Gallent, M. C. Figueiredo, A. J. Göttle, F. Calle-Vallejo and M. T. M. Koper, Advances and challenges in understanding the electrocatalytic conversion of carbon dioxide to fuels, *Nat. Energy*, 2019, **4**, 732–745.
15 C. Wang, Z. Sun, Y. Zheng and Y. H. Hu, Recent progress in visible light photocatalytic conversion of carbon dioxide, *J. Mater. Chem. A*, 2019, **7**, 865–887.
16 C. Jiang, S. J. A. Moniz, A. Wang, T. Zhang and J. Tang, Photoelectrochemical devices for solar water splitting-materials and challenges, *Chem. Soc. Rev.*, 2017, **46**, 4645–4660.
17 D. Voiry, H. S. Shin, K. P. Loh and M. Chhowalla, Low-dimensional catalysts for hydrogen evolution and $CO_2$ reduction, *Nat. Rev. Chem.*, 2018, **2**, 0105.
18 B. Qiao, A. Wang, X. Yang, L. F. Allard, Z. Jiang, Y. Cui, J. Liu, J. Li and T. Zhang, Single-atom catalysis of CO oxidation using $Pt_1/FeO_x$, *Nat. Chem.*, 2011, **3**, 634–641.
19 Y. Xiong, W. Sun, Y. Han, P. Xin, X. Zheng, W. Yan, J. Dong, J. Zhang, D. Wang and Y. Li, Cobalt single atom site catalysts with ultrahigh metal loading for enhanced aerobic oxidation of ethylbenzene, *Nano Res.*, 2021, **14**, 2418–2423.
20 Y. Xiong, W. Sun, P. Xin, W. Chen, X. Zheng, W. Yan, L. Zheng, J. Dong, J. Zhang, D. Wang and Y. Li, Gram-Scale Synthesis of High-Loading Single-Atomic-Site Fe Catalysts for Effective Epoxidation of Styrene, *Adv. Mater.*, 2020, **32**, 2000896.
21 B. H. Lee, S. Park, M. Kim, *et al.*, Reversible and cooperative photoactivation of single-atom $Cu/TiO_2$ photocatalysts, *Nat. Mater.*, 2019, **18**, 620–626.
22 J. H. Wang, M. S. Yin, Q. Zhang, F. Cao, Y. Xing, Q. Zhao, Y. Wang, W. Xu, W. Wu and M. Wu, Single-Atom Fe-$N_4$ sites promote the triplet-energy transfer process of g-$C_3N_4$ for the photooxidation, *J. Catal.*, 2021, **404**, 89–95.
23 H. Ou, D. Wang and Y. Li, How to select effective electrocatalysts: Nano or single atom?, *Nano Select*, 2021, **2**, 492–511.

 

24 Q. N. Zhan, T. Y. Shuai, H. M. Xu, C. J. Huang, Z. J. Zhang and G. R. Li, Syntheses and applications of single-atom catalysts for electrochemical energy conversion reactions, *Chin. J. Catal.*, 2023, **47**, 32–66.
25 Q. Sun, C. Jia, Y. Zhao and C. Zhao, Single atom-based catalysts for electrochemical $CO_2$ reduction, *Chin. J. Catal.*, 2022, **43**, 1547–1597.
26 L. Wang, S. Lyu and S. Li, *In situ* observation of structural evolution of single-atom catalysts: From synthesis to catalysis, *ChemPhysMater*, 2024, **3**, 24–35.
27 M. Zhong, K. Tran, Y. Min, C. Wang, Z. Wang, C. T. Dinh, P. D. Luna, Z. Yu, A. S. Rasouli, P. Brodersen, S. Sun, O. Voznyy, C. S. Tan, M. Askerka, F. Che, M. Liu, A. Seifitokaldani, Y. Pang, S.-C. Lo, A. Ip, Z. Ulissi and E. H. Sargent, Accelerated discovery of $CO_2$ electrocatalysts using active machine learning, *Nature*, 2020, **581**, 178–183.
28 Y. Yang, S. Louisia, S. Yu, J. Jin, I. Roh, C. Chen, M. V. Fonseca Guzman, J. Feijóo, P. C. Chen, H. Wang, C. J. Pollock, X. Huang, Y. T. Shao, C. Wang, D. A. Muller, H. D. Abruña and P. Yang, Operando studies reveal active Cu nanograins for $CO_2$ electroreduction, *Nature*, 2023, **614**, 262–269.
29 W. Fang, W. Guo, R. Lu, Y. Yan, X. Liu, D. Wu, F. M. Li, Y. Zhou, C. He, C. Xia, H. Niu, S. Wang, Y. Liu, Y. Mao, C. Zhang, B. You, Y. Pang, L. Duan, X. Yang, F. Song, T. Zhai, G. Wang, X. Guo, B. Tan, T. Yao, Z. Wang and B. Y. Xia, Durable $CO_2$ conversion in the proton-exchange membrane system, *Nature*, 2024, **626**, 86–91.
30 Y. Xiao, H. T. Zhang and M. T. Zhang, Heterobimetallic NiFe Complex for Photocatalytic $CO_2$ Reduction: United Efforts of NiFe Dual Sites, *J. Am. Chem. Soc.*, 2024, **146**, 28832–28844.
31 Z. Wu, J. Liu, B. Mu, X. Xu, W. Sheng, W. Tao and Z. Li, Machine-Learning assisted screening of double metal catalysts for $CO_2$ electroreduction to $CH_4$, *Appl. Surf. Sci.*, 2024, **648**, 159027.
32 Y. Li, S. Wang, Z. Lv, Z. Wang, Y. Zhao, Y. Xie, Y. Xu, L. Qian, Y. Yang, Z. Zhao and J. Zhang, Transforming the synthesis of carbon nanotubes with machine learning models and automation, *Matter*, 2025, **8**, 101913.
33 V. Sumaria, T. B. Rawal, Y. F. Li, D. Sommer, J. Vikoren, R. J. Bondi, M. Rupp, A. Prasad and D. Prasad, Machine Learning, Density Functional Theory, and Experiments to Understand the Photocatalytic Reduction of $CO_2$ on CuPt/$TiO_2$, *J. Phys. Chem. C*, 2024, **128**, 14247–14258.
34 J. Liu, Y. Cai, R. Song, S. Ding, Z. Lyu, Y.-C. Chang, H. Tian, X. Zhang, D. Du, W. Zhu, Y. Zhou and Y. Lin, Recent progress on single-atom catalysts for $CO_2$ electroreduction, *Mater. Today*, 2021, **48**, 95–114.
35 X. F. Ziang Shang, G. Chen, R. Qin and Y. Han, Recent Advances on Single-Atom Catalysts for Photocatalytic $CO_2$ Reduction, *Small*, 2023, **19**, 2304975.
36 W. Hu, H. Yang and C. Wang, Progress in photocatalytic $CO_2$ reduction based on single-atom catalysts, *RSC Adv.*, 2023, **13**, 20889–20908.
37 J. Lin, B. Qiao, J. Liu, Y. Huang, A. Wang, L. Li, W. Zhang, L. F. Allard, X. Wang and T. Zhang, Design of a Highly Active Ir/Fe$(OH)_x$ Catalyst: Versatile Application of Pt-Group Metals for the Preferential Oxidation of Carbon Monoxide, *Angew. Chem., Int. Ed.*, 2012, **51**, 2920–2924.
38 B. J. O'Neill, D. H. K. Jackson, J. Lee, C. Canlas, P. C. Stair, C. L. Marshall, J. W. Elam, T. F. Kuech, J. A. Dumesic and G. W. Huber, Catalyst Design with Atomic Layer Deposition, *ACS Catal.*, 2015, **5**, 1804–1825.
39 S. Sun, G. Zhang, N. Gauquelin, N. Chen, J. Zhou, S. Yang, W. Chen, X. Meng, D. Geng, *et al.*, Single-atom catalysis using Pt/graphene achieved through atomic layer deposition, *Sci. Rep.*, 2013, **3**, 1775.
40 L. Zhang, Z. J. Zhao and J. Gong, Nanostructured Materials for Heterogeneous Electrocatalytic $CO_2$ Reduction and their Related Reaction Mechanisms, *Angew. Chem., Int. Ed.*, 2017, **56**, 11326.
41 T. Ouyang, H. H. Huang, J. W. Wang, D. C. Zhong and T. B. Lu, A Dinuclear Cobalt Cryptate as a Homogeneous Photocatalyst for Highly Selective and Efficient Visible-Light Driven $CO_2$ Reduction to CO in $CH_3CN/H_2O$ Solution, *Angew. Chem.*, 2017, **129**, 756–761.
42 C. Zhu, S. Fu, Q. Shi, D. Du and Y. Lin, Single-atom electrocatalysts, *Angew. Chem., Int. Ed.*, 2017, **56**, 13944.
43 Y. Wang, P. Han, X. Lv, L. Zhang and G. Zheng, Defect and Interface Engineering for Aqueous Electrocatalytic $CO_2$ Reduction, *Joule*, 2018, **12**, 2551–2582.
44 N. Corbin, J. Zeng, K. Williams and K. Manthiram, Heterogeneous molecular catalysts for electrocatalytic $CO_2$ reduction, *Nano Res.*, 2019, **12**, 2093–2125.
45 Z. Yang, W. Gao and Q. Jiang, A machine learning scheme for the catalytic activity of alloys with intrinsic descriptors, *J. Mater. Chem. A*, 2020, **8**, 17507–17515.
46 K. Tran and Z. W. Ulissi, Active learning across intermetallics to guide discovery of electrocatalysts for $CO_2$ reduction and $H_2$ evolution, *Nat. Catal.*, 2018, **1**, 696–703.
47 M. Zhong, K. Tran, Y. Min, C. Wang, Z. Wang, C. T. Dinh, P. De Luna, Z. Yu, A. S. Rasouli, P. Brodersen, S. Sun, O. Voznyy, C. S. Tan, M. Askerka, F. Che, M. Liu, A. Seifitokaldani, Y. Pang, S. C. Lo, A. Ip, Z. Ulissi and E. H. Sargent, Accelerated discovery of $CO_2$ electrocatalysts using active machine learning, *Nature*, 2020, **581**, 178–183.
48 W. Gao, Y. Chen, B. Li, S. P. Liu, X. Liu and Q. Jiang, Determining the adsorption energies of small molecules with the intrinsic properties of adsorbates and substrates, *Nat. Commun.*, 2020, **11**, 1196.
49 X. Ma, Z. Li, L. E. Achenie and H. Xin, Machine-Learning-Augmented Chemisorption Model for $CO_2$ Electroreduction Catalyst Screening, *J. Phys. Chem. Lett.*, 2015, **6**, 3528–3533.
50 X. Wan, Z. Zhang, H. Niu, Y. Yin, C. Kuai, J. Wang, C. Shao and Y. Guo, Machine-Learning-Accelerated Catalytic Activity Predictions of Transition Metal Phthalocyanine Dual-Metal-Site Catalysts for $CO_2$ Reduction, *J. Phys. Chem. Lett.*, 2021, **12**, 6111–6118.

51 S. Özsoysal, B. Oral and R. Yıldırım, Analysis of photocatalytic $CO_2$ reduction over MOFs using machine learning, *J. Mater. Chem. A*, 2024, **12**, 5748–5759.
52 Q. Yang, L. Zhao, R. Bao, Y. Fan, J. Zhou, D. Rong, H. Zhou and D. Zhang, Interpretable machine learning-assisted advanced exergy optimization for carbon-neutral olefins production, *Renewable Sustainable Energy Rev.*, 2025, **208**, 115027.
53 H. Sun and J. Y. Liu, Advancing $CO_2$RR with O-Coordinated Single-Atom Nanozymes: A DFT and Machine Learning Exploration, *ACS Catal.*, 2024, **14**, 14021–14030.
54 L.-H. Mou, J. Du, Y. Li, J. Jiang and L. Chen, Effective Screening Descriptors of Metal-Organic Framework-Supported Single-Atom Catalysts for Electrochemical $CO_2$ Reduction Reactions: A Computational Study, *ACS Catal.*, 2024, **14**, 12947–12955.
55 R. Ding, J. Chen, Y. Chen, J. Liu, Y. Bando and X. Wang, Unlocking the potential: machine learning applications in electrocatalyst design for electrochemical hydrogen energy transformation, *Chem. Soc. Rev.*, 2024, **53**, 11390–11461.
56 M. Sun and B. Huang, Direct Machine Learning Predictions of $C_3$ Pathways, *Adv. Energy Mater.*, 2024, **14**, 2400152.
57 J. Ock, S. Badrinarayanan, R. Magar, A. Antony and A. B. Farimani, Multimodal language and graph learning of adsorption configuration in catalysis, *Nat. Mach. Intell.*, 2024, **6**, 1501–1511.
58 M. Ren, X. Guo, S. Zhang and S. Huang, Design of Graphdiyne and Holey Graphyne-Based Single Atom Catalysts for $CO_2$ Reduction With Interpretable Machine Learning, *Adv. Funct. Mater.*, 2023, **33**, 2213543.
59 X. Bai, Y. Li, Y. Xie, Q. Chen, X. Zhang and J. R. Li, High-throughput screening of $CO_2$ cycloaddition MOF catalyst with an explainable machine learning model, *Green Energy Environ.*, 2025, **10**, 132–138.
60 L. Wang, H. Chen, L. Yang, J. Li, Y. Li and X. Wang, Single-atom catalysts property prediction via Supervised and Self-Supervised pre-training models, *Chem. Eng. J.*, 2024, **487**, 150626.
61 Q. Zhu, Y. Gu, X. Liang, X. Wang and J. Ma, A Machine Learning Model to Predict $CO_2$ Reduction Reactivity and Products Transferred from Metal-Zeolites, *ACS Catal.*, 2022, **12**, 12336–12348.
62 A. S. Varela, N. Ranjbar Sahraie, J. Steinberg, W. Ju, H. S. Oh and P. Strasser, Metal-Doped Nitrogenated Carbon as an Efficient Catalyst for Direct $CO_2$ Electroreduction to CO and Hydrocarbons, *Angew. Chem.*, 2015, **127**, 10908–10912.
63 R. Guo, C. Guo, Z. Bi, H. Zhang, N. Lv, B. Xi, G. Hu and J. Xu, The single atom Fe loaded catalytic membrane for effective peroxymonosulfate activation and pollution degradation, *Appl. Catal., B*, 2024, **356**, 124243.
64 A. V. Bukhtiyarov, M. A. Panafidin, I. P. Prosvirin, N. S. Smirnova, P. V. Markov, G. N. Baeva, I. S. Mashkovsky, G. O. Bragina, C. Rameshan, E. Yu. Gerasimov, Y. V. Zubavichus, V. I. Bukhtiyarov and A. Yu. Stakheev, Deliberate control of the structure-specific active sites in PdIn bimetallic catalysts using adsorbate induced segregation effects, *Appl. Surf. Sci.*, 2023, **608**, 155–086.
65 G. A. Naikoo, F. Arshad, I. U. Hassan, F. B. Omar, M. M. Tambuwala, M. Mustaqeem and T. A. Saleh, Trends in bimetallic nanomaterials and methods for fourth-generation glucose sensors, *Trends Anal. Chem.*, 2023, **162**, 117042.
66 S. K. Lahiri, C. Zhang, M. Sillanpää and L. Liu, NiO@$SiO_2$ photo-catalyst prepared by ion-exchange method for fast elimination of reactive dyes from wastewater, *Mater. Today Chem.*, 2022, **23**, 100–677.
67 A. Kowalczyk, A. Borcuch, M. Michalik, M. Rutkowska, B. Gil, Z. Sojka, P. Indyka and L. Chmielarz, MCM-41 modified with transition metals by template ion-exchange method as catalysts for selective catalytic oxidation of ammonia to dinitrogen, *Microporous Mesoporous Mater.*, 2017, **240**, 9–21.
68 V. Andrei, I. Roh, J. A. Lin, J. Lee, Y. Shan, C. K. Lin, S. Shelton, E. Reisner and P. Yang, Perovskite-driven solar $C_2$ hydrocarbon synthesis from $CO_2$, *Nat. Catal.*, 2025, 137–146.
69 K. Maeda, D. An, R. Kuriki, D. Lu and O. Ishitani, Graphitic carbon nitride prepared from urea as a photocatalyst for visible-light carbon dioxide reduction with the aid of a mononuclear ruthenium(II) complex, *J. Org. Chem.*, 2018, **14**, 1806–1812.
70 W. Zhang, Z. Jin and Z. Chen, Rational-Designed Principles for Electrochemical and Photoelectrochemical Upgrading of $CO_2$ to Value-Added Chemicals, *Adv. Sci.*, 2022, **9**, 2105204.
71 X. Tao, Y. Wang, J. Qu, Y. Zhao, R. Li and C. Li, Achieving selective photocatalytic $CO_2$ reduction to CO on bismuth tantalum oxyhalogen nanoplates, *J. Mater. Chem. A*, 2021, **9**, 19631–19636.
72 X. M. You, B. Xu, H. Zhou, H. Qiao, X. Lv, Z. Huang, J. Pang, L. Yang, P. F. Liu, X. Guan, H. G. Yang, X. Wang and Y. F. Yao, Ultrahigh Bifunctional Photocatalytic $CO_2$ Reduction and $H_2$ Evolution by Synergistic Interaction of Heteroatomic Pt-Ru Dimerization Sites, *ACS Nano*, 2024, **18**, 9403–9412.
73 A. Fujishima and K. Honda, Electrochemical photolysis of water at a semiconductor electrode, *Nature*, 1972, **238**, 37–38.
74 M. Halmann, Photoelectrochemical reduction of aqueous carbon dioxide on p-type gallium phosphide in liquid junction solar cells, *Nature*, 1978, **275**, 115–116.
75 J. Xia, N. Karjule, B. Mondal, J. Qin, M. Volokh, L. Xing and M. Shalom, Design of melem-based supramolecular assemblies for the synthesis of polymeric carbon nitrides with enhanced photocatalytic activity, *J. Mater. Chem. A*, 2021, **9**, 17855–17864.
76 J. Wu, Y. Huang, W. Ye and Y. Li, $CO_2$ Reduction: From the Electrochemical to Photochemical Approach, *Adv. Sci.*, 2017, **4**, 1700194.
77 H. Zhang, Y. Wang, S. Zuo, W. Zhou, J. Zhang and X. W. D. Lou, Isolated Cobalt Centers on $W_{18}O_{49}$

 

Nanowires Perform as a Reaction Switch for Efficient $CO_2$ Photoreduction, *Chem. Soc.*, 2021, **143**, 2173–2177.
78 Y. Li, S. Wang, X. Wang, Y. He, Q. Wang, Y. Li, M. Li, G. Yang, J. Yi, H. Lin, D. Huang, L. Li, H. Chen and J. Ye, Facile top-down strategy for direct metal atomization and coordination achieving a high turnover number in $CO_2$ Photoreduction, *J. Am. Chem. Soc.*, 2020, **142**, 19259–19267.
79 C. Feng, T. T. Bo, P. Maity, S. W. Zuo, W. Zhou, K. W. Kuang, O. F. Mohammed and H. Zhang, Regulating Photocatalytic $CO_2$ Reduction Kinetics through Modification of Surface Coordination Sphere, *Adv. Funct. Mater.*, 2024, **34**, 2309761.
80 Y. Zhang, B. Johannessen, P. Zhang, J. Gong, J. Ran and S. Z. Qiao, Reversed Electron Transfer in Dual Single Atom Catalyst for Boosted Photoreduction of $CO_2$, *Adv. Mater.*, 2023, **35**, 2306923.
81 H. Haroon and Q. Xiang, Single-Atom based Metal-Organic Framework Photocatalysts for Solar-Fuel Generation, *Small*, 2024, **20**, 2401389.
82 Y. Wang, L. Liao, G. Zhu, W. Xie, Q. Zhou, F. Yu, H. Zhou and H. Zhou, Metal-nitrogen coordinated single atomic photocatalysts for solar energy conversion, *Coord. Chem. Rev.*, 2025, **523**, 216254.
83 Q. Yang, H. Liu, Y. Lin, D. Su, Y. Tang and L. Chen, Atomically Dispersed Metal Catalysts for the Conversion of $CO_2$ into High-Value $C_{2+}$ Chemicals, *Adv. Mater.*, 2024, **36**, 2310912.
84 Y. Zheng, W. Li, J. Ju, J. Jiang, L. Zhang, H. Jiang, Y. Hu and C. Li, Oxygen vacancy mediated Pd-SA/$TiO_2$ single-atom catalyst created via ultra-fast one-step synthesis for enhanced $CO_2$ photoreduction, *J. Colloid Interface Sci.*, 2025, **683**, 280–290.
85 B. Rhimi, M. Zhou, Z. Yan, X. Cai and Z. Jiang, Cu-Based Materials for Enhanced $C_{2+}$ Product Selectivity in Photo-/Electro-Catalytic $CO_2$ Reduction: Challenges and Prospects, *Nano-Micro Lett.*, 2024, **16**, 64.
86 Y. Luo, X. Wang, F. Gao, L. Jiang, D. Wang and H. Pan, From Single Atom Photocatalysts to Synergistic Photocatalysts: Design Principles and Applications, *Adv. Funct. Mater.*, 2024, 2418427.
87 W. Lyu, Y. Liu, J. Zhou, D. Chen, X. Zhao, R. Fang, F. Wang and Y. Li, Modulating the Reaction Configuration by Breaking the Structural Symmetry of Active Sites for Efficient Photocatalytic Reduction of Low-concentration $CO_2$, *Angew. Chem., Int. Ed.*, 2023, **62**, e202310733.
88 Z. W. Huang, K. Q. Hu, X. B. Li, Z. N. Bin, Q. Y. Wu, Z. H. Zhang, Z. J. Guo, W. S. Wu, Z. F. Chai, L. Mei and W. Q. Shi, Thermally Induced Orderly Alignment of Porphyrin Photoactive Motifs in Metal–Organic Frameworks for Boosting Photocatalytic $CO_2$ Reduction, *J. Am. Chem. Soc.*, 2023, **145**, 18148–18159.
89 L. Cheng, H. Yin, C. Cai, J. Fan and Q. Xiang, Single Ni Atoms Anchored on Porous Few–Layer g–$C_3N_4$ for Photocatalytic $CO_2$ Reduction: The Role of Edge Confinement, *Small*, 2020, **16**, 2002411.
90 P. Zhang, X. Zhan, L. Xu, X. Fu, T. Zheng, X. Yang, Q. Xu, D. Wang, D. Qi, T. Sun and J. Jiang, Mass production of a single-atom cobalt photocatalyst for high-performance visible-light photocatalytic $CO_2$ reduction, *J. Mater. Chem. A*, 2021, **9**, 26286–26297.
91 A. Wang, J. Li and T. Zhang, Heterogeneous single-atom catalysis, *Nat. Rev. Chem.*, 2018, **2**, 65–81.
92 P. Zhang, X. Zhan, L. Xu, X. Fu, T. Zheng, X. Yang, Q. Xu, D. Wang, D. Qi, T. Sun and J. Jiang, Mass production of a single-atom cobalt photocatalyst for high-performance visible-light photocatalytic $CO_2$ reduction, *J. Mater. Chem. A*, 2021, **9**, 26286–26297.
93 J. Lee, G. I. N. Waterhouse, Y. Mao, Z. Wang, E. Zhu, J. Low, S. P. Chai and L. L. Tan, Lead-free halide perovskites and Bi-BTC frameworks: Engineering S-scheme heterojunctions for photocatalytic $CO_2$ conversion, *Appl. Catal., B*, 2025, **365**, 124942.
94 J. He, X. Wang, P. Feng, Y. Zhou, K. Wang, B. Zou and M. Zhu, Isostructural phase transition-induced piezoelectricity in all-inorganic perovskite $CsPbBr_3$ for catalytic $CO_2$ reduction, *Appl. Catal., B*, 2024, **355**, 124186.
95 Y. Feng, D. Chen, M. Niu, Y. Zhong, Z. He, S. Ma, K. Yuan, H. Ding, K. Lv, L. Guo, W. Zhang and M. Ma, Ligand free synthesis of atomically dispersed Cu doping ultrathin $Cs_3Bi_2Br_9$ for efficient photoreduction $CO_2$ with high CO selectivity, *Appl. Catal., B*, 2025, **365**, 124931.
96 Z. L. Liu, Y. F. Mu, X. R. Li, Y. X. Feng, M. Zhang and T. B. Lu, Constructing strong built-in electric field in lead-free halide-perovskite-based heterojunction to boost charge separation for efficient $CO_2$ photoreduction, *Appl. Catal., B*, 2025, **366**, 125012.
97 H. Sun, Z. Lin, R. Tang, Y. Liang, S. Zou, X. Zhang, K. Chen, R. Zheng and J. Huang, Enhanced solar urea synthesis from $CO_2$ and nitrate waste via oxygen vacancy mediated-$TiO_x$ support lead-free perovskite, *Appl. Catal., B*, 2025, **360**, 124511.
98 Q. Lu, J. Rosen, Y. Zhou, G. S. Hutchings, Y. C. Kimmel, J. G. Chen and F. Jiao, A selective and efficient electrocatalyst for carbon dioxide reduction, *Nat. Commun.*, 2014, **5**, 32–42.
99 B. Zhang and J. Zhang, Rational design of Cu-based electrocatalysts for electrochemical reduction of carbon dioxide, *Energy Chem.*, 2017, **26**, 1050–1066.
100 J. He, N. J. J. Johnson, A. Huang and C. P. Berlinguette, Electrocatalytic Alloys for $CO_2$ Reduction, *ChemSusChem*, 2018, **11**, 48–57.
101 Q. Hao, Q. Tang, H. X. Zhong, J. Z. Wang, D. X. Liu and X. B. Zhang, Fully exposed nickel clusters with electron-rich centers for high-performance electrocatalytic $CO_2$ reduction to CO, *Sci. Bull.*, 2022, **67**, 1477–1485.
102 S. Liu, H. B. Yang, S. F. Hung, J. Ding, W. Cai, L. Liu, J. Gao, X. Li, X. Ren, Z. Kuang, Y. Huang, T. Zhang and B. Liu, Elucidating the Electrocatalytic $CO_2$ Reduction Reaction over a Model Single–Atom Nickel Catalyst, *Angew. Chem., Int. Ed.*, 2019, **59**, 798–803.

103 H. Gu, J. Wu and L. Zhang, Recent advances in the rational design of single-atom catalysts for electrochemical $CO_2$ reduction, *Nano Res.*, 2022, **15**, 9747–9763.
104 N. Qiu, J. Li, H. Wang and Z. Zhang, Emerging dual-atomic-site catalysts for electrocatalytic $CO_2$ reduction, *Sci. China Mater.*, 2022, **65**, 3302–3323.
105 Y. Li, Z. He, F. Wu, S. Wang, Y. Cheng and S. Jiang, Defect engineering of high-loading single-atom catalysts for electrochemical carbon dioxide reduction, *Mater. Rep. Energy*, 2023, **3**, 100197.
106 D. Gao, T. Liu, G. Wang and X. Bao, Structure Sensitivity in Single-Atom Catalysis toward $CO_2$ Electroreduction, *ACS Energy Lett.*, 2021, **6**, 713–727.
107 Y. E. Kim, Y. N. Ko, B. S. An, J. Hong, Y. E. Jeon, H. J. Kim, S. Lee, J. Lee and W. Lee, Atomically Dispersed Nickel Coordinated with Nitrogen on Carbon Nanotubes to Boost Electrochemical $CO_2$ Reduction, *Energy Lett.*, 2023, **8**, 3288–3296.
108 Y. Wang, Y. Liu, W. Liu, J. Wu, Q. Li, Q. Feng, Z. Chen, X. Xiong, D. Wang and Y. Lei, Regulating the coordination structure of metal single atoms for efficient electrocatalytic $CO_2$ reduction, *Energy Environ. Sci.*, 2020, **13**, 4609–4624.
109 S. Yang, H. An, S. Arnouts, H. Wang, X. Yu, J. de. Ruiter, S. Bals, T. Altantzis, B. M. Weckhuysen and W. V. D. Stam, Halide-guided active site exposure in bismuth electrocatalysts for selective $CO_2$ conversion into formic acid, *Nat. Catal.*, 2023, **6**, 796–806.
110 J. Feng, L. Zhang, S. Liu, L. Xu, X. Ma, X. Tan, L. Wu, Q. Qian, T. Wu, J. Zhang, X. Sun and B. Han, Modulating adsorbed hydrogen drives electrochemical $CO_2$-to-$C_2$ products, *Nat. Commun.*, 2023, **14**, 4615.
111 Z. Jin, M. Yang, Y. Dong, X. Ma, Y. Wang, J. Wu, J. Fan, D. Wang, R. Xi, X. Zhao, T. Xu, J. Zhao, *et al.*, Atomic Dispersed Hetero-Pairs for Enhanced Electrocatalytic $CO_2$ Reduction, *Nano-Micro Lett.*, 2024, **16**, 4.
112 Y. Cao, S. Chen, S. Bo, W. Fan, J. Li, C. Jia, Z. Zhou, Q. Liu, L. Zheng and F. Zhang, Single Atom Bi Decorated Copper Alloy Enables C-C Coupling for Electrocatalytic Reduction of $CO_2$ into $C_{2+}$ Products, *Angew. Chem.*, 2023, **135**, e202303048.
113 F. Cai, D. Gao, H. Zhou, G. Wang, T. He, H. Gong, S. Miao, F. Yang, J. Wang and X. Bao, Electrochemical promotion of catalysis over Pd nanoparticles for $CO_2$ reduction, *Chem. Sci.*, 2017, **8**, 2569–2573.
114 Y. Quan, R. Yu, J. Zhu, A. Guan, X. Lv, C. Yang, S. Li, J. Wu and G. Zheng, Efficient carboxylation of styrene and carbon dioxide by single-atomic copper electrocatalyst, *J. Colloid Interface Sci.*, 2021, **601**, 378–384.
115 J. Rosen, G. S. Hutchings, Q. Lu, R. V. Forest, A. Moore and J. Feng, Electrodeposited Zn Dendrites with Enhanced CO Selectivity for Electrocatalytic $CO_2$ Reduction, *ACS Catal.*, 2015, **5**, 4586–4591.
116 Y. Chen and M. W. Kanan, Tin Oxide Dependence of the $CO_2$ Reduction Efficiency on Tin Electrodes and Enhanced Activity for Tin/Tin Oxide Thin-Film Catalysts, *J. Am. Chem. Soc.*, 2012, **134**, 1986–1989.
117 H. Mistry, R. Reske, Z. Zeng, Z. J. Zhao, J. Greeley, P. Strasser and B. R. Cuenya, Exceptional Size-Dependent Activity Enhancement in the Electroreduction of $CO_2$ over Au Nanoparticles, *Chem. Soc.*, 2014, **136**, 16473–16476.
118 C. Kim, T. Eom, M. S. Jee, H. Jung, H. Kim, B. K. Min and Y. J. Hwang, Insight into Electrochemical $CO_2$ Reduction on Surface-Molecule-Mediated Ag Nanoparticles, *ACS Catal.*, 2017, **7**, 779–785.
119 J. M. Spurgeon and B. Kumar, A comparative technoeconomic analysis of pathways for commercial electrochemical $CO_2$ reduction to liquid products, *Energy Environ. Sci.*, 2018, **11**, 1536.
120 C. Kim, F. Dionigi, V. Beermann, X. Wang, T. Möller and P. Strasser, Alloy Nanocatalysts for the Electrochemical Oxygen Reduction (ORR) and the Direct Electrochemical Carbon Dioxide Reduction Reaction ($CO_2$RR), *Adv. Mater.*, 2019, **31**, 1805617.
121 W. Gao, Y. Xu, L. Fu, X. Chang and B. Xu, Experimental evidence of distinct sites for $CO_2$-to-CO and CO conversion on Cu in the electrochemical $CO_2$ reduction reaction, *Nat. Catal.*, 2023, **6**, 885–894.
122 Q. Wang, X. Yang, H. Zang, C. Liu, J. Wang, N. Yu, L. Kuai, Q. Qin and B. Geng, InBi Bimetallic Sites for Efficient Electrochemical Reduction of $CO_2$ to HCOOH, *Small*, 2023, **19**, 2303172.
123 A. R. Woldu, A. G. Yohannes, Z. Huang, P. Kennepohl, D. Astruc, L. Hu and X. C. Huang, Experimental and Theoretical Insights into Single Atoms, Dual Atoms, and Sub-Nanocluster Catalysts for Electrochemical $CO_2$ Reduction ($CO_2$RR) to High-Value Products, *Adv. Mater.*, 2024, **36**, 2414169.
124 H. Dai, T. Song, X. Yue, S. Wei, F. Li, Y. Xu, S. Shu, Z. Cui, C. Wang, J. Gu and L. Duan, Cu single-atom electrocatalyst on nitrogen-containing graphdiyne for $CO_2$ electroreduction to $CH_4$, *Chin. J. Catal.*, 2024, **64**, 123–132.
125 B. Wang, M. Wang, Z. Fan, C. Ma, S. Xi, L. Y. Chang, M. Zhang, N. Ling, Z. Mi, S. Chen, W. R. Leow, J. Zhang, D. Wang and Y. Lum, Nanocurvature-induced field effects enable control over the activity of single-atom electrocatalysts, *Nat. Commun.*, 2024, **15**, 1719.
126 R. Purbia, S. Y. Choi, C. H. Woo, J. Jeon, C. Lim, D. K. Lee, J. Y. Choi, H.-S. Oh and J. M. Baik, Highly selective and low-overpotential electrocatalytic CO2 reduction to ethanol by Cu-single atoms decorated N-doped carbon dots, *Appl. Catal., B*, 2024, **345**, 123694.
127 S. Cui, C. Yu, X. Tan, W. Li, Y. Zhang and J. Qiu, A tandem catalyst with high $CO_2$ capture capability to achieve a promoted $CO_2$-to-$CH_4$ electrochemical conversion, *Chem. Eng. J.*, 2023, **470**, 144083.
128 J. Ding, B. H. Yang, X. L. Ma, S. Liu, W. Liu, Q. Mao, Y. Huang, J. Li, T. Zhang and B. Liu, A tin-based tandem electrocatalyst for $CO_2$ reduction to ethanol with 80% selectivity, *Nat. Energy*, 2023, **8**, 1386–1394.

 

129 Y. Wang, S. L. Marquard, D. Wang, C. Dares and T. J. Meyer, Single-Site, Heterogeneous Electrocatalytic Reduction of $CO_2$ in water as the Solvent, *ACS Energy Lett.*, 2017, **2**, 1395–1399.
130 S. Baskaran and Y. Jung, $Mo_2CS_2$-MXene supported single-atom catalysts for efficient and selective $CO_2$ electrochemical reduction, *Appl. Surf. Sci.*, 2022, **592**, 153339.
131 D. Zhao, Z. Chen, W. Yang, S. Liu, X. Zhang, Y. Yu, W. C. Cheong, L. Zheng, F. Ren, G. Ying, *et al.*, MXene ($Ti_3C_2$) vacancy-confined single-atom catalyst for efficient functionalization of $CO_2$, *J. Am. Chem. Soc.*, 2019, **141**, 4086–4093.
132 W. Liu, H. Li, P. Ou, J. Mao, L. Han, J. Song, J. Luo and H. L. Xin, Isolated Cu-Sn diatomic sites for enhanced electroreduction of $CO_2$ to CO, *Nano Res.*, 2023, **16**, 8729–8736.
133 L. Zhang, J. Feng, L. Wu, X. Ma, X. Song, S. Jia, X. Tan, X. Jin, Q. Zhu, X. Kang, J. Ma, *et al.*, Oxophilicity-controlled $CO_2$ electroreduction to $C_{2+}$ alcohols over Lewis acid metal-doped $Cu^{\delta+}$ catalysts, *J. Am. Chem. Soc.*, 2023, **145**, 21945–21954.
134 X. Su, Y. Sun, L. Jin, L. Zhang, Y. Yang, P. Kerns, B. Liu, S. Li and J. He, Hierarchically porous Cu/Zn bimetallic catalysts for highly selective $CO_2$ electroreduction to liquid $C_2$ products, *Appl. Catal., B*, 2020, **269**, 118800.
135 G. Chen, J. Fu, B. Liu, C. Cai, H. Li, Z. Zhang, K. Liu, Z. Lin and M. Liu, Passivation of Cu nanosheet dissolution with $Cu^{2+}$-containing electrolytes for selective electroreduction of $CO_2$ to $CH_4$, *Environ. Sci.:Nano*, 2022, **9**, 3312–3317.
136 Z. Xu, Y. Xie and Y. Wang, Pause electrolysis for acidic $CO_2$ reduction on 3-dimensional Cu, *Mater. Rep. Energy*, 2023, **3**, 100173.
137 M. Fan, J. E. Huang, R. K. Miao, Y. Mao, P. Ou, F. Li, X. Y. Li, Y. Cao, Z. Zhang, J. Zhang, *et al.*, Cationic-group-functionalized electrocatalysts enable stable acidic $CO_2$ electrolysis, *Nat. Catal.*, 2023, **6**, 763–772.
138 S. Cao, H. Chen, X. Wei, J. Li, C. Yang, Z. Chen, S. Wei, S. Liu, Z. Wang and X. Lu, Asymmetric coordination engineering of active centers in MXene-based single atom catalysts for high-performance $ECO_2RR$, *Carbon*, 2024, **225**, 119094.
139 S. Chen, T. Luo, X. Li, K. Chen, Q. Wang, J. Fu, K. Liu, C. Ma, Y.-R. Lu, H. Li, K. S. Menghrajani, C. Liu, S. A. Maier, T.-S. Chan and M. Liu, Design of reaction-driven active configuration for enhanced $CO_2$ electroreduction, *Nano Energy*, 2024, **128**, 109873.
140 Z. Lv, C. Wang, Y. Liu, R. Liu, F. Zhang, X. Feng, W. Yang and B. Wang, Improving $CO_2$-to-$C_2$ Conversion of Atomic CuFONC Electrocatalysts through F, O-Codrived Optimization of Local Coordination Environment, *Adv. Energy Mater.*, 2024, **14**, 2400057.
141 S. Yang, H. Wang, Y. Xiong, M. Zhu, J. Sun, M. Jiang, P. Zhang, J. Wei, Y. Xing, Z. Tie and Z. Jin, Ultrafast Thermal Shock Synthesis and Porosity Engineering of 3D Hierarchical Cu–Bi Nanofoam Electrodes for Highly Selective Electrochemical $CO_2$, *Nano Lett.*, 2023, **23**, 10140–10147.
142 Z. Wang, J. Yang, Z. Song, M. Lu, W. Wang, Z. Ren and Z. Chen, Reprogramming the Microenvironment of Cobalt Phthalocyanine by a Targeted Multifunctional π-Conjugated Modulator Enables Concerted $CO_2$ Electroreduction, *ACS Catal.*, 2024, **14**, 8138–8147.
143 J. Lei and T. Zhu, Impact of Potential and Active-Site Environment on Single-Iron-Atom-Catalyzed Electrochemical $CO_2$ Reduction from Accurate Quantum Many-Body Simulations, *ACS Catal.*, 2024, **14**, 3933–3942.
144 A. Kumar, M. Ubaidullah, P. V. Pham and R. K. Gupta, Three-dimensional macro-structures of graphene-based materials for emerging heterogeneous electrocatalysis: Concepts, syntheses, principles, applications, and perspectives, *Chem. Eng. J.*, 2024, **499**, 156664.
145 J. M. Gracia, F. F. Prinsloo and J. W. Niemantsverdriet, Mars-van Krevelen-like Mechanism of CO Hydrogenation on an Iron Carbide Surface, *Catal. Lett.*, 2009, **133**, 257–261.
146 J. Chai, R. Pestman, W. Chen, N. Donkervoet, A. I. Dugulan, Z. Men, P. Wang and E. J. M. Hensen, Isotopic Exchange Study on the Kinetics of Fe Carburization and the Mechanism of the Fischer-Tropsch Reaction, *ACS Catal.*, 2022, **12**, 2877–2887.
147 L. Brübach, D. Hodonj and P. Pfeifer, Kinetic Analysis of $CO_2$ Hydrogenation to Long-Chain Hydrocarbons on a Supported Iron Catalyst, *Ind. Eng. Chem. Res.*, 2022, **61**, 1644–1654.
148 Y. Sun, G. Yang, M. Xu, J. Xu and Z. Sun, A simple coupled ANNs–RSM approach in modeling product distribution of Fischer–Tropsch synthesis using a microchannel reactor with Ru–promoted $Co/Al_2O_3$ catalyst, *Int. J. Energy Res.*, 2020, **44**, 1046–1061.
149 Y. Wang, J. Hu, X. Zhang, A. Yusuf, B. Qi, H. Jin, Y. Liu, J. He, Y. Wang, G. Yang and Y. Sun, Kinetic Study of Product Distribution Using Various Data-Driven and Statistical Models for Fischer-Tropsch Synthesis, *ACS Omega*, 2021, **6**, 27183–27199.
150 Q. Zhang, L. Guo and Z. Hao, CO hydrogenation on $M_1/W_6S_8$ (M = Co and Ni) single-atom catalysts: Competition between $C_2$ hydrocarbons and methanol synthesis pathways, *Mol. Catal.*, 2019, **464**, 10–21.
151 X. Wang, X. P. Fu, W. Z. Yu, C. Ma, C. J. Jia and R. Si, Synthesis of a ceria-supported iron–ruthenium oxide catalyst and its structural transformation from subnanometer clusters to single atoms during the Fischer–Tropsch synthesis reaction, *Inorg. Chem. Front.*, 2017, **4**, 2059–2067.